The 30 May 1998 Spencer, South Dakota, Storm. Part I: The Structural Evolution and Environment of the Tornadoes

CURTIS R. ALEXANDER

School of Meteorology, University of Oklahoma, Norman, Oklahoma, and Center for Severe Weather Research, Boulder, Colorado

JOSHUA WURMAN

Center for Severe Weather Research, Boulder, Colorado

(Manuscript received 28 January 2004, in final form 2 July 2004)

ABSTRACT

On the evening of 30 May 1998 atmospheric conditions across southeastern South Dakota led to the development of organized moist convection including several supercells. One such supercell was tracked by both a Weather Surveillance Radar-1988 Doppler (WSR-88D) from Sioux Falls, South Dakota (KFSD), and by a Doppler On Wheels (DOW) mobile radar. This supercell remained isolated for an hour and a half before being overtaken by a developing squall line. During this time period the supercell produced at least one strong and one violent tornado, the latter of which passed through Spencer, South Dakota, despite the absence of strong low-level environmental wind shear. The two tornadoes were observed both visually and with the DOW radar at ranges between 1.7 and 12.9 km. The close proximity to the tornadoes permitted the DOW radar to observe tornado-scale structures on the order of 35 to 100 m, while the nearest WSR-88D only resolved the parent mesocyclone in the supercell. The DOW observations revealed a persistent Doppler velocity couplet and associated ring reflectivity signature at the tip of the hook echo.

The DOW radar data contained tornado strength winds over 35 m s^{-1} within 100 m AGL approximately 180 s prior to both the first spotter report and visual confirmation of the first tornado associated with this supercell. Following the formation of the second tornado, the DOW radar observations revealed a tornado-strength Doppler velocity couplet within 150 m AGL between two separate tornado tracks determined by a National Weather Service (NWS) damage survey. Based upon the DOW Doppler velocity data it appears that the second and third damage tracks from this supercell are produced from a single tornado.

The time–height evolution of the Doppler velocity couplet spanning both tornadoes revealed a gradual increase in vertical vorticity across each tornado's core region within a few hundred meters AGL from near 0.2 to over 2.0 s^{-1} over a 45-min period. A corresponding reduction in vertical vorticity was observed aloft especially near 1000 m AGL where vorticity values decreased from near 1.0 to about 0.5 s^{-1} during this same time interval. The shear across the Doppler velocity couplet appears to undergo strengthening both at the surface and aloft during both tornadoes. An oscillatory fluctuation in the near-surface shear across the tornado core developed during the second tornado, with peak shear values as high as 206 m s^{-1}, Doppler velocities over 106 m s^{-1}, and peak ground-relative wind speeds reaching 118 m s^{-1}. The period of this intensity oscillation appears to be around 120 s and was most prominent just prior to and during the passage of the tornado through Spencer. Coincident with the tornado passage through Spencer was a rapid descending of the reflectivity eye in the core of the tornado. A detailed comparison of surveyed tornado damage and radar-calculated tornado winds in Spencer is discussed in Part II.

1. Introduction

Considerable research has focused on characterizing the structure and intensity of tornadoes. In the late 1960s and early 1970s laboratory models were developed to study the evolution of tornado vortices (Ward 1972; Church et al. 1979; Church and Snow 1993). As computer processing speed and storage capacity increased, the laboratory models gave way to numerical models of tornadoes in the late 1970s and the 1980s (Rotunno 1977, 1979, 1984). These numerical simulations of tornado vortices continued through the 1990s and expanded upon the study of tornado dynamics in an attempt to determine the theoretical limit to wind speeds and the finescale structure of tornadoes (Fiedler and Rotunno 1986; Fiedler 1998; Lewellen 1993; Lewellen et al. 1997; Lewellen et al. 2000).

The 1980s also saw the first attempts to measure directly tornado winds in the field. Instrument packages containing anemometers were deployed in the fore-

Corresponding author address: Curtis Alexander, School of Meteorology, University of Oklahoma, 100 East Boyd Street, #1442, Norman, OK 73019.
E-mail: curtisa@ou.edu

casted path of tornadoes. These attempts resulted in little success, as the packages were either destroyed, or more often, the tornado did not pass over them. More recently these efforts have met with more success (Winn et al. 2000; Samaras 2004; Wurman and Samaras 2004). Mobile Doppler radars were deployed near tornadoes starting in the early 1990s (Bluestein et al. 1993). Doppler velocity measurements from these tornadoes yielded more significant results in an attempt to gauge tornado wind speeds. By the mid- to late 1990s, several other mobile radar platforms were developed and deployed in the field to directly observe tornadoes, yielding even more frequent and detailed high-resolution observations of tornadoes (Bluestein et al. 1995; Bluestein and Pazmany 2000; Wurman et al. 1996, 2002; Wurman 1996; Wurman and Gill 2000; Lee and Wurman 2004, manuscript submitted to *J. Atmos. Sci.*). These newer mobile radar platforms included the Doppler On Wheels (DOW; Wurman et al. 1997; Wurman 2001), which mapped two- and three-dimensional wind fields in tornadoes for the first time. A DOW has been used in this work to document the two- and three-dimensional evolution of tornadoes near Spencer, South Dakota. Comparisons of radar-measured winds and observed damage in Spencer are the subject of the second part of this study (Wurman and Alexander 2005, hereafter Part II).

2. Synoptic environment

The synoptic environment on the afternoon and evening of 30 May 1998 was conducive to the development of severe thunderstorms across the northern plains of the United States. By 0000 UTC 31 May 1998 (1900 local time 30 May 1998), a southwest-to-northeast-oriented 300-mb jet streak containing winds in excess of 50 m s^{-1} was approaching South Dakota from the southwest. At the same time, another 300-mb jet streak, also containing winds in excess of 51 m s^{-1}, was centered just north of the Great Lakes and was moving away from South Dakota. The juxtaposition of these two jet maximums placed eastern South Dakota in the left-exit region of the approaching jet, and near the right-entrance region of the departing jet (Fig. 1a). While the along-stream variation in wind speed along each jet axis was not extremely high, eastern South Dakota appeared to be in a region of enhanced upper-level divergence. This was likely a factor in the widespread initiation of deep moist convection.

At 500 mb, a positively tilted trough was positioned upstream from South Dakota along an axis from central Canada to northern California. Across South Dakota, winds were about 23 m s^{-1} from the west-southwest with an air temperature around −12°C at 500 mb (Fig. 1b). At 700 mb, South Dakota was near the northern edge of a strongly capped environment with an air temperature near 10°C that increased southward to 15°C in western Kansas (Fig. 2a). The 850-mb level contained a strong north–south temperature gradient across the northern plains, with temperatures in North Dakota near 12°C increasing to 25°C in western Nebraska (Fig. 2b). This enhanced temperature gradient was evidence of a synoptic-scale front positioned across the northern plains. A trough axis was also located over eastern South Dakota at 850 mb, although the maximum in 850-mb winds was along an axis displaced well to the south and east of South Dakota from southern Wisconsin southwestward to central Kansas (Fig. 2b).

The surface map valid at 0000 31 May 1998 showed a well-defined cold front extending east to west across central South Dakota (Fig. 3). Air temperatures across the cold front decreased by 11°C into southern North Dakota. At the same time, a sharp dryline was oriented north to south extending from a triple-point intersection with the cold front in central South Dakota southward through central Nebraska. The air mass behind the dryline contained surface dewpoints near or below 0°C. In the warm and moist sector across southeastern South Dakota, surface temperatures were around 27°C with dewpoints near 21°C. Surface winds were generally light from the south, but given these surface conditions and strong westerly midlevel flow, this produced deep-layer shear in excess of 17 m s^{-1}, which was supportive for the development and maintenance of severe convective storms (Weisman and Klemp 1982). These favorable conditions were also enhanced by high values of convective available potential energy (CAPE) and low values of convective inhibition (CIN) over southeastern South Dakota resulting from deep low-level moisture and relatively cool midlevel temperatures (Moncrieff and Miller 1976; Colby 1984).

An Omaha, Nebraska, sounding from 0000 UTC 31 May 1998, which was the nearest upper-air observation in the warm and moist sector, contained over 3700 J kg^{-1} of mixed-layer CAPE in a moderately capped environment with a CIN of −47 J kg^{-1} (Fig. 4a). The 700–500-mb lapse rates exceeded 8°C km^{-1}. Farther north in southeast South Dakota, midlevel temperatures were slightly cooler and surface dewpoints were slightly higher, resulting in mixed-layer CAPE estimates exceeding 4000 J kg^{-1}, and the 700-mb temperatures were slightly cooler, likely resulting in less CIN (USDOC 1998). The LCL height was near 800 mb in Omaha, and with smaller surface dewpoint depressions farther to the north, the LCL height in southeastern South Dakota was likely below 800 mb and more supportive of tornado formation (Rasmussen and Blanchard 1998). The low-level shear was not extremely high across southeastern South Dakota because the low-level jet was displaced to the south and east, and this was a condition that did not appear to favor the development of violent tornadoes (Fig. 4b). However, all other synoptic-scale and mesoscale ingredients were present for a significant severe weather event including tornadic supercells.

The air mass across southeastern South Dakota was capped with a layer of warm air contributing to convective inhibition residing just above potentially unsta-

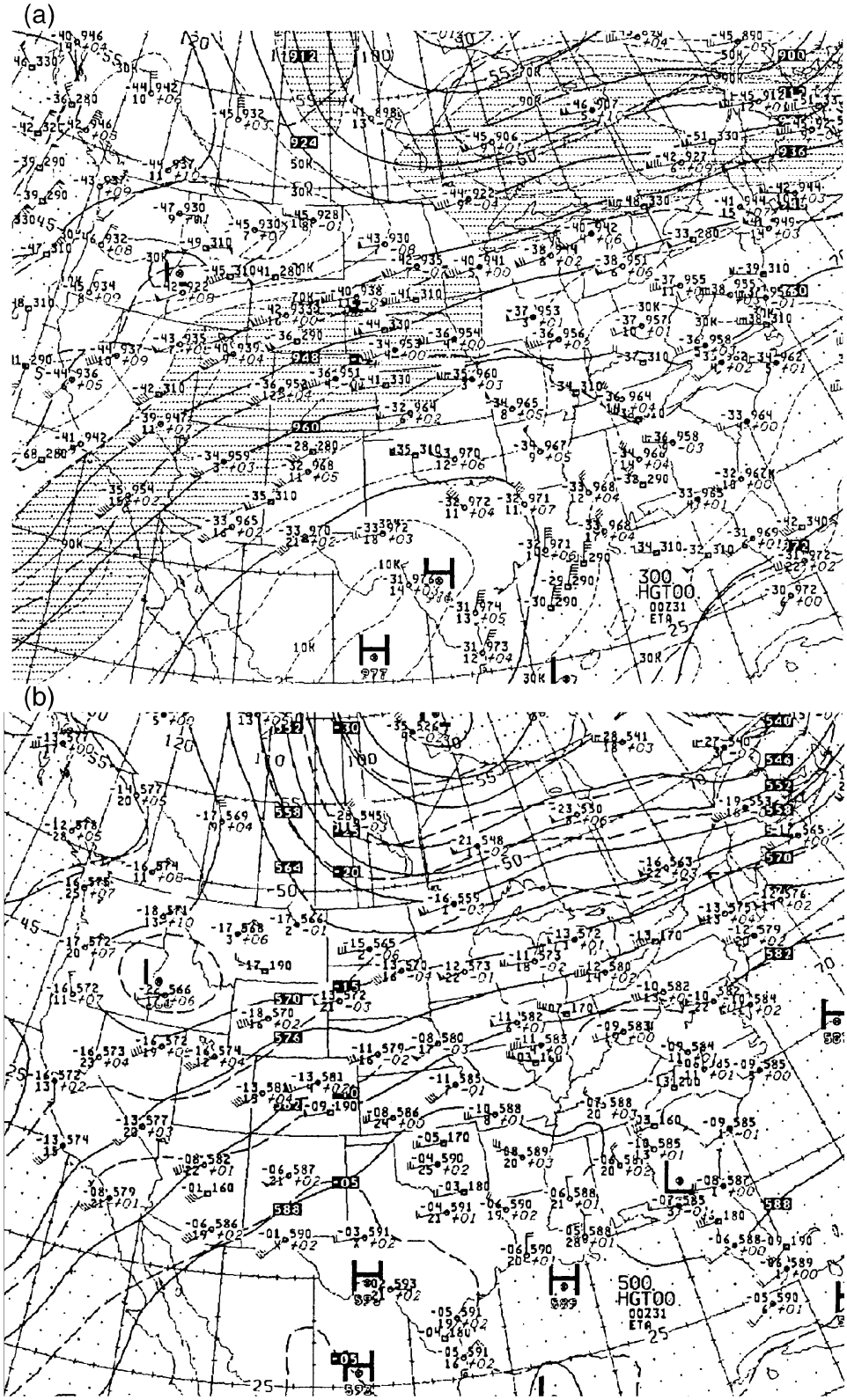

FIG. 1. Synoptic analysis from upper-air observations valid at 0000 UTC 31 May 1998 showing (a) 300-mb heights (solid lines in dam) and isotachs (dashed lines in kt) and (b) 500-mb heights (solid lines in dam) and temperatures (dashed lines in °C).

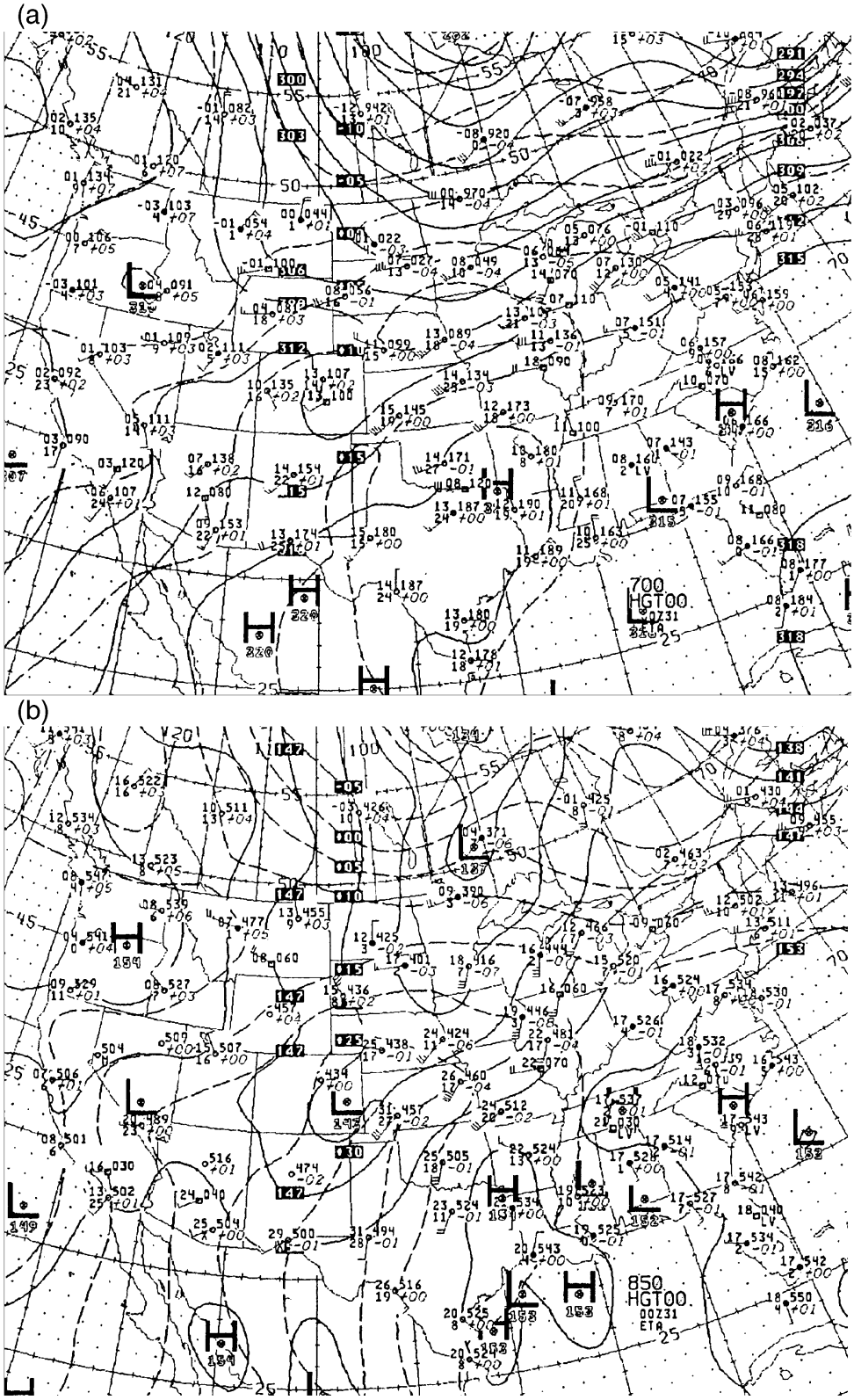

FIG. 2. Synoptic analysis from upper-air observations valid at 0000 UTC 31 May 1998 showing (a) 700-mb heights (solid lines in dam) and temperatures (dashed lines in °C) and (b) 850-mb heights (solid lines in dam) and temperatures (dashed lines in °C).

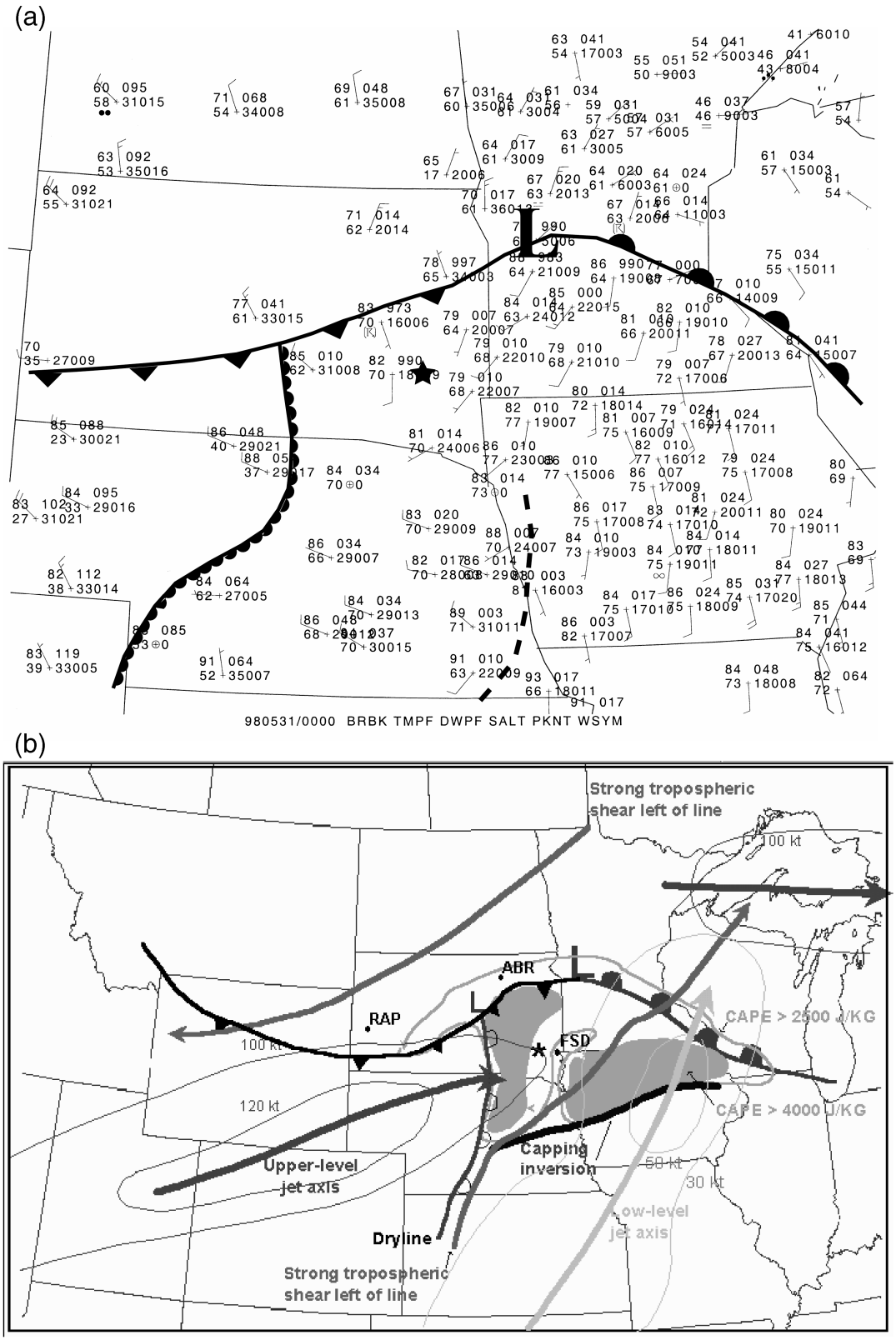

FIG. 3. (a) Mesoscale analysis of surface observations including temperatures (°F), dewpoint (°F), pressure (mb), wind speed (kt), and wind direction at 0000 UTC 31 May 1998. The position of surface features, including a cold front, warm front, dryline, convergence zone (dashed line), and Spencer, SD (star), are shown. (b) Composite synoptic features at 2300 UTC 30 May 1998 (reproduced from USDOC 1998) including regions with CAPE in excess of 4000 J kg^{-1} (shaded regions).

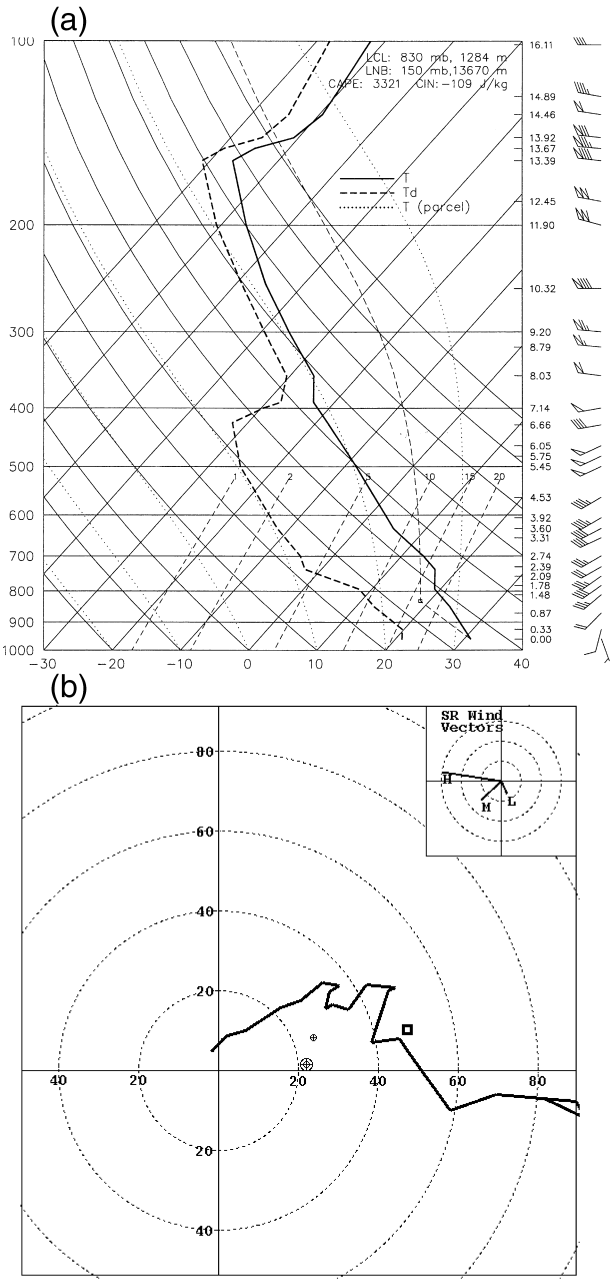

FIG. 4. Omaha, NE, sounding valid at 0000 UTC 31 May 1998 with (a) skew *T*–log*p* diagram representing thermodynamic characteristics of the warm moist sector and (b) hodograph depicting the kinematic characteristics of the environment including estimated storm-relative wind vectors.

ble air near the surface. However, synoptic-scale lift from low-level geostrophic warm-air advection, midlevel differential geostrophic cyclonic vorticity advection, and the aforementioned upper-level divergence in the vicinity of the jet maximums aided mesoscale lift along the advancing cold front and dryline. All of these ingredients helped initiate deep moist convection around 2300 UTC 30 May near the dryline and cold-front intersection. Several other isolated thunderstorms developed southward along the dryline by 2300 UTC including a storm about 100 km west-northwest of Spencer. By 0030 UTC 31 May, this storm organized into a supercell with a well-defined midlevel mesocyclone.

While there is some uncertainty as to the exact evolution of events between 0100 and 0200 UTC, intermittent spotter reports and a damage survey conducted from the National Weather Service (NWS) indicated that five separate tornadoes were responsible for damage observed from the supercell that tracked across parts of Hanson and McCook Counties in southeastern South Dakota including the town of Spencer. The analysis presented herein shows that fewer tornadoes, in fact, occurred.

3. DOW data postprocessing

The data analyzed and discussed herein were collected with the Doppler On Wheels 3 (DOW3) radar (Wurman et al. 1997; Wurman 2001). The DOW3 used 3-cm transmissions with 250-kW peak power and had a beamwidth of 0.93°. Pulse pair processing converted received signals to typical radar moments resulting in radar reflectivity, Doppler velocity, etc., and short integration times resulted in azimuthal oversampling by factors of about 2 or 3. Full specifications of DOW3 can be found in Wurman (2001). Scanning was conducted mainly in a sector volume mode through about 140° of azimuth and at elevations of 0.5°, 1°, 2°, 3°, 4°, 5°, 6°, 8°, 10°, and 14° elevation. Range gating resulted in 37-m-range resolution and the DOW's 0.93° beamwidth resulted in cross-beam resolution that ranged from about 23 to 81 m (oversampled to result in data every 12 to 40 m) during the second deployment. However, the diameter of the radar beam at genesis was as high as 230 m (oversampled to provide 115-m resolution).

Several stages of data quality control were implemented to ensure accurate analysis of the tornado wind field and surrounding region. The radar data, initially in PC Integrated Radar Data Acquisition System II (PIRAQ-II) field format, was translated into Doppler Radar Data Exchange (DORADE) format, and then edited using the SOLO software package (Nettleton et al. 1993; Oye et al. 1995). Each gate in every ray of each elevation scan had the uncalibrated reflectivity and Doppler velocity moments thresholded against the normalized coherent power (NCP). Range gates where the NCP value fell below 0.25 were deleted, as this was an indication of insufficient signal-to-noise ratio for accurate measurements of velocity. Data were also deleted where significant ground clutter contamination was detected as evidenced by Doppler velocities near 0 m s^{-1} and uncalibrated reflectivity values exceeding about 0 dB from obviously nonmeteorological targets such as buildings, power lines, power poles, etc. Doppler velocities were then dealiased around the appropriate multiple of the Nyquist interval (either ± 24 or ± 32 m s^{-1}).

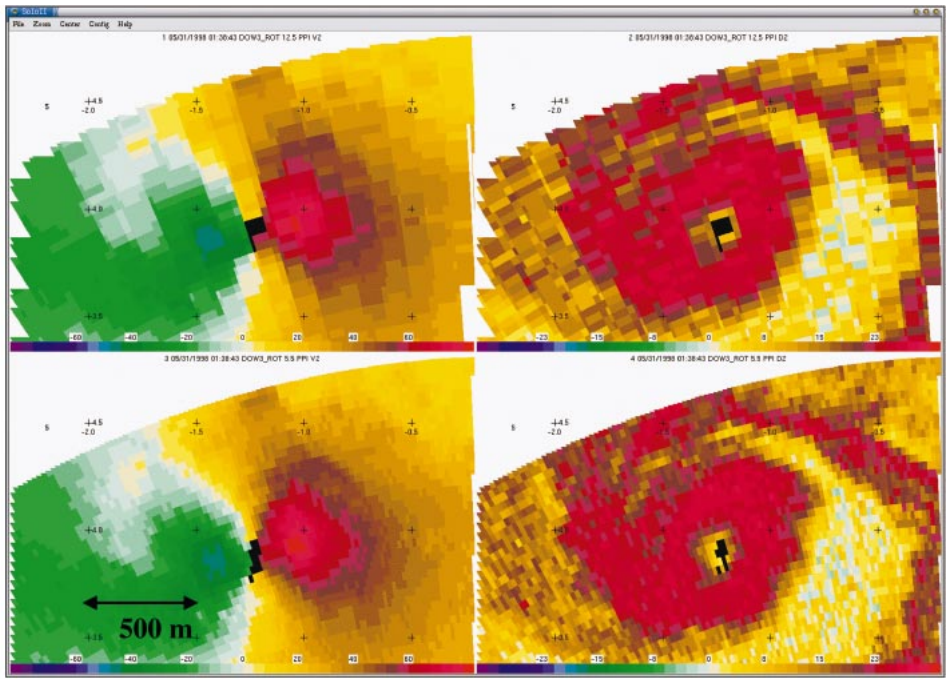

FIG. 5. Edited Doppler velocity (m s^{-1}) and uncalibrated reflectivity (dB) fields from DOW3 (a) before applying the beam angle correction and (b) after applying the beam angle correction.

The final step of quality control was unique to this radar dataset. A data acquisition processing limitation in DOW3 in 1998 produced infrequent updates of the reported azimuth and elevation angles of the radar beam. This problem produced a symptomatic error whereby every consecutive two or three beams contained the same pointing angle. The error was corrected by knowing the antenna rotation rate, the pulse repetition time (PRT), the number of pulses per beam integration, and assuming that the antenna moved at a constant angular velocity during the beam integration period (0.01 s). The product of these three quantities yielded the appropriate angular separation between adjacent beams. A two-pass ten-ray running-mean correction filter was developed to correct ray azimuth and elevation angles in each tilt. Application of this filter to the radar data resulted in the appropriate beam positions in each sweep (Fig. 5).

Following the quality control procedures, it was necessary to rotate the radar data from a truck-relative to a ground-relative coordinate system in a manner similar to Wurman and Gill (2000). The location of DOW3 was determined from onboard GPS information and navigational notes, resulting in an estimated position accurate to within about 5 m. The orientation of the truck relative to north was obtained by comparing the ground clutter reflectivity returns from the lowest elevation of several volumes and a U.S. Geological Survey (USGS) map of the local region. Strong radar returns from the surrounding network of roads, power lines, and vegetation provided sufficient information when compared with computerized USGS maps to determine the orientation of DOW3 to within about 0.1° as estimated from the agreement among orientations determined from many clutter features. The resulting total positioning error was about 10 m for sample volumes over Spencer, and this was several times smaller than the size of a sample volume and less than the typical spacing between buildings.

4. Radar observations of the Spencer, South Dakota, supercell

Between 0030 and 0100 UTC, the supercell northwest of Spencer developed a low-level mesocyclone as seen by KFSD, the Weather Surveillance Radar-1988 Doppler (WSR-88D) from Sioux Falls, South Dakota (Fig. 6). The KFSD mesocyclone detection algorithm (MDA) began tracking a mesocyclone associated with this storm shortly after 0045 UTC (Table 1). Range folding in the Doppler velocity field produced from severe convection located farther to the northwest likely prevented earlier detection of a mesocyclone in this storm from the KFSD MDA. This supercell maintained an east-southeastward motion with an average heading of around 110° and forward speed of about 13 m s^{-1} between 0045 and 0135 UTC. The gate-to-gate shear across the mesocyclone increased from about 30 m s^{-1} at 0046 UTC to a peak of 68 m s^{-1} at 0106 UTC. The strong rear-flank downdraft was evident in the extended area of strong inbound (relative to KFSD) Doppler velocities to the south of the mesocyclone at 0101 and 0106 UTC

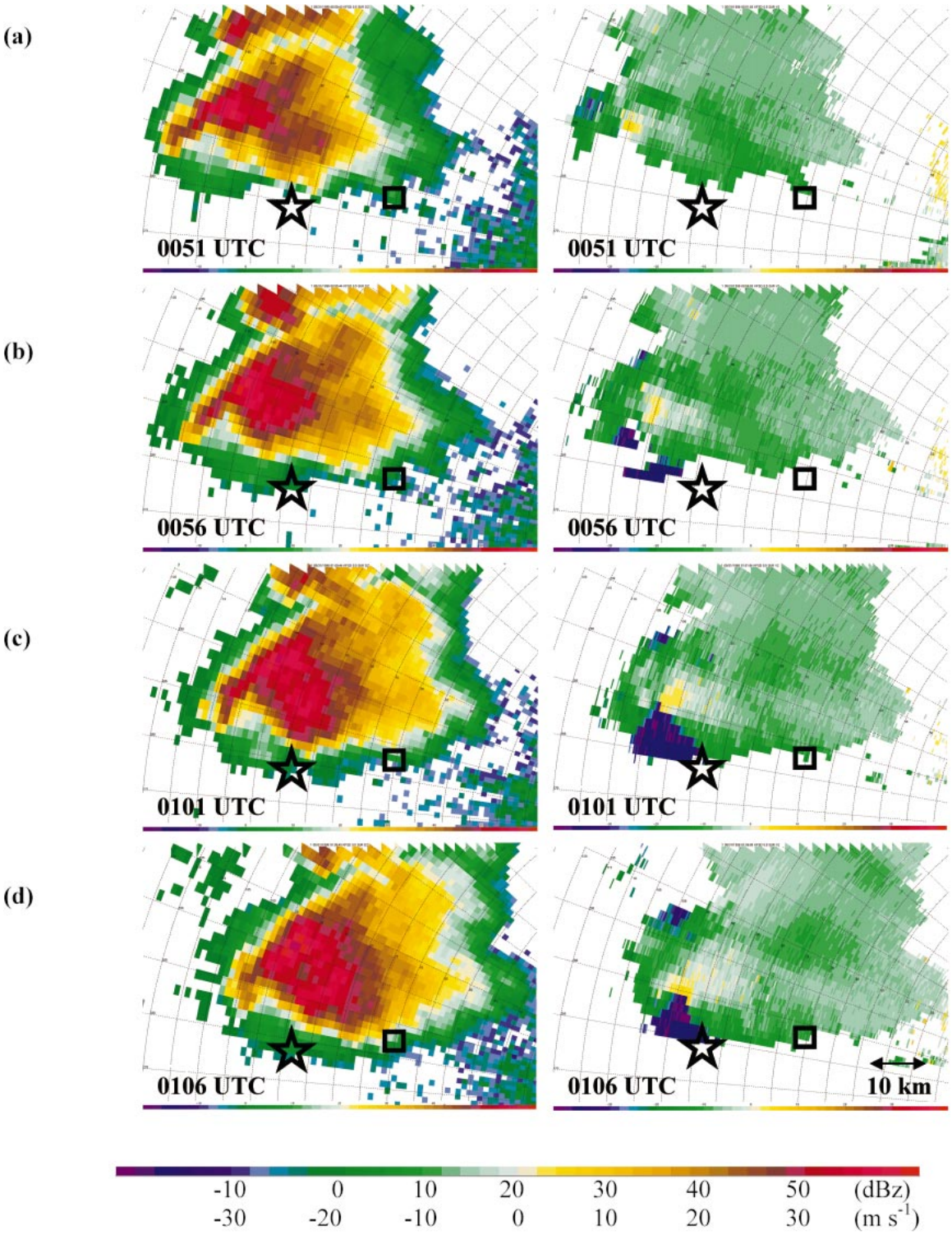

FIG. 6. The 0.5° elevation scan of a supercell from KFSD showing both (left) base reflectivity and (right) edited Doppler velocity at (a) 0051, (b) 0056, (c) 0101, and (d) 0106 UTC. The star and square represent the locations of DOW3 during its first deployment and Spencer, respectively.

TABLE 1. DOW3 Doppler velocity couplet attributes, KFSD MDA, and TVS algorithms between 0015 and 0215 UTC for the Spencer supercell and associated tornadoes. The range, height AGL, and peak shear of the couplet in the lowest DOW3 scan nearest to the times of MDA and TVS algorithm executions are shown for reference. The range, height AGL, and magnitude of the peak shear in the MDA and TVS are listed from the algorithms. The MDA classifications include no significant shear (None), 2D uncorrelated shear (UNC), 3D correlated shear (COR), and mesocyclone detection (MESO). The TVS algorithm classification is either no detection (None) or TVS. Boldfaced row indicates the time that the tornado was in Spencer.

	DOW3			KFSD MDA				KFSD TVS			
Time (UTC)	Range (km)	Height (km)	Shear (s^{-1})	Class	Range (km)	Height (km)	Shear (s^{-1})	Class	Range (km)	Height (km)	Shear (s^{-1})
0015:29	N/A	N/A	N/A	None	None	None	None	None	None	None	None
0020:37	N/A	N/A	N/A	None	None	None	None	None	None	None	None
0025:39	N/A	N/A	N/A	None	None	None	None	None	None	None	None
0030:49	N/A	N/A	N/A	None	None	None	None	None	None	None	None
0035:41	N/A	N/A	N/A	None	None	None	None	None	None	None	None
0040:41	N/A	N/A	N/A	None	None	None	None	None	None	None	None
0045:42	N/A	N/A	N/A	MESO	111.1	5.4	0.023	None	None	None	None
0050:43	N/A	N/A	N/A	UNC	109.3	5.3	0.034	None	None	None	None
0055:44	N/A	N/A	N/A	None	None	None	None	None	None	None	None
0100:44	N/A	N/A	N/A	MESO	96.3	6.3	0.014	None	None	None	None
0105:45	11.5	0.15	0.17	MESO	94.5	1.4	0.036	TVS	96.3	4.7	0.016
0110:44	9.6	0.12	0.59	MESO	92.6	1.3	0.041	None	None	None	None
0115:42	6.1	0.09	1.43	MESO	87.0	1.2	0.041	TVS	85.2	6.8	0.015
0123:47	5.2	0.04	0.75	MESO	79.6	1.0	0.038	TVS	79.6	5.1	0.021
0128:55	4.9	0.14	0.38	MESO	74.1	1.0	0.054	None	None	None	None
0133:56	1.7	0.02	0.69	MESO	68.5	5.7	0.053	TVS	84.1	2.3	0.038
0138:57	**3.8**	**0.05**	**0.54**	**MESO**	**68.5**	**5.4**	**0.053**	**TVS**	**70.4**	**2.1**	**0.042**
0143:59	8.2	0.10	0.49	MESO	64.8	7.1	0.040	TVS	68.5	3.1	0.024
0148:59	N/A	N/A	N/A	MESO	61.1	7.8	0.034	None	None	None	None
0154:01	N/A	N/A	N/A	MESO	55.6	7.6	0.029	TVS	55.6	7.5	0.021
0159:00	N/A	N/A	N/A	MESO	51.9	3.4	0.027	TVS	53.7	3.3	0.016
0204:01	N/A	N/A	N/A	MESO	51.9	5.5	0.022	None	None	None	None
0209:02	N/A	N/A	N/A	MESO	46.3	4.5	0.021	None	None	None	None
0214:02	N/A	N/A	N/A	MESO	40.7	3.9	0.018	None	None	None	None

(Lemon and Doswell 1979). The tornado vortex signature algorithm (TVS) from KFSD generated its first TVS detection in this supercell just prior to 0106 UTC (Table 1). The KFSD MDA reached a maximum in shear intensity for this supercell between 0111 and 0116 UTC before briefly weakening.

Archived level-II KFSD radar data were unavailable for the time period between 0111 and 0129 UTC when the radar power was transferred from a commercial to a generator source (USDOC 1998). The mesocyclone strength index (MSI) as reported by Carey et al. (2003) increases significantly during this data gap, and then remains approximately constant until after 0145 UTC. The first spotter report of a funnel cloud occurred at 0055 UTC on 31 May followed by the first report of a tornado at 0108 UTC about 8 miles northeast of Mitchell (USDOC 1998).

During the 1-h period from approximately 0100 to 0200 UTC on 31 May the DOW3 mobile radar was following this supercell as part of the Radar Observation of Thunderstorms and Tornadoes Experiment 1998 (ROTATE-98) field project (Wurman 1999). DOW3 first deployed along Highway 38 almost due south of Fulton, South Dakota, between 0103 and 0122 UTC, beginning 5 min before the first spotter-reported tornado (Fig. 7). The DOW radar collected high-resolution reflectivity and Doppler velocity measurements of the tornadic portion of the supercell that eventually passed through Spencer. These radar measurements resolved the detailed structure of the hook echo including the tip where a Doppler velocity couplet often appeared collocated with a minimum in the reflectivity field surrounded by an annulus of higher reflectivity values (Fig. 8). It is important to note that the DOW reflectivity values presented herein are uncalibrated; therefore, only the relative intensities are meaningful. Furthermore, since the DOW was deployed very near to high-reflectivity regions of the supercell and tornado, receiver saturation resulted in spuriously low reflectivity values near the radar (Dowell et al. 2005). The Doppler velocity couplet contained ground-relative velocities over 35 m s^{-1} and a core diameter of about 150 m at about 75 m AGL at 0104:41 UTC. The core diameter grew in subsequent scans. Video taken from this DOW deployment site indicated the formation of a tornado around 0107 UTC, with the first indication of a debris cloud at the ground concurring with the aforementioned spotter report. Therefore it appears that a tornado strength and scale circulation was at the surface approximately 3 min prior to the first visual evidence of a tornado. By 0108 UTC a condensation funnel extended from storm base to the ground before being enveloped in a column of dust by 0115 UTC (Fig. 9). There were few structures to corroborate the gap in the NWS damage survey track, and

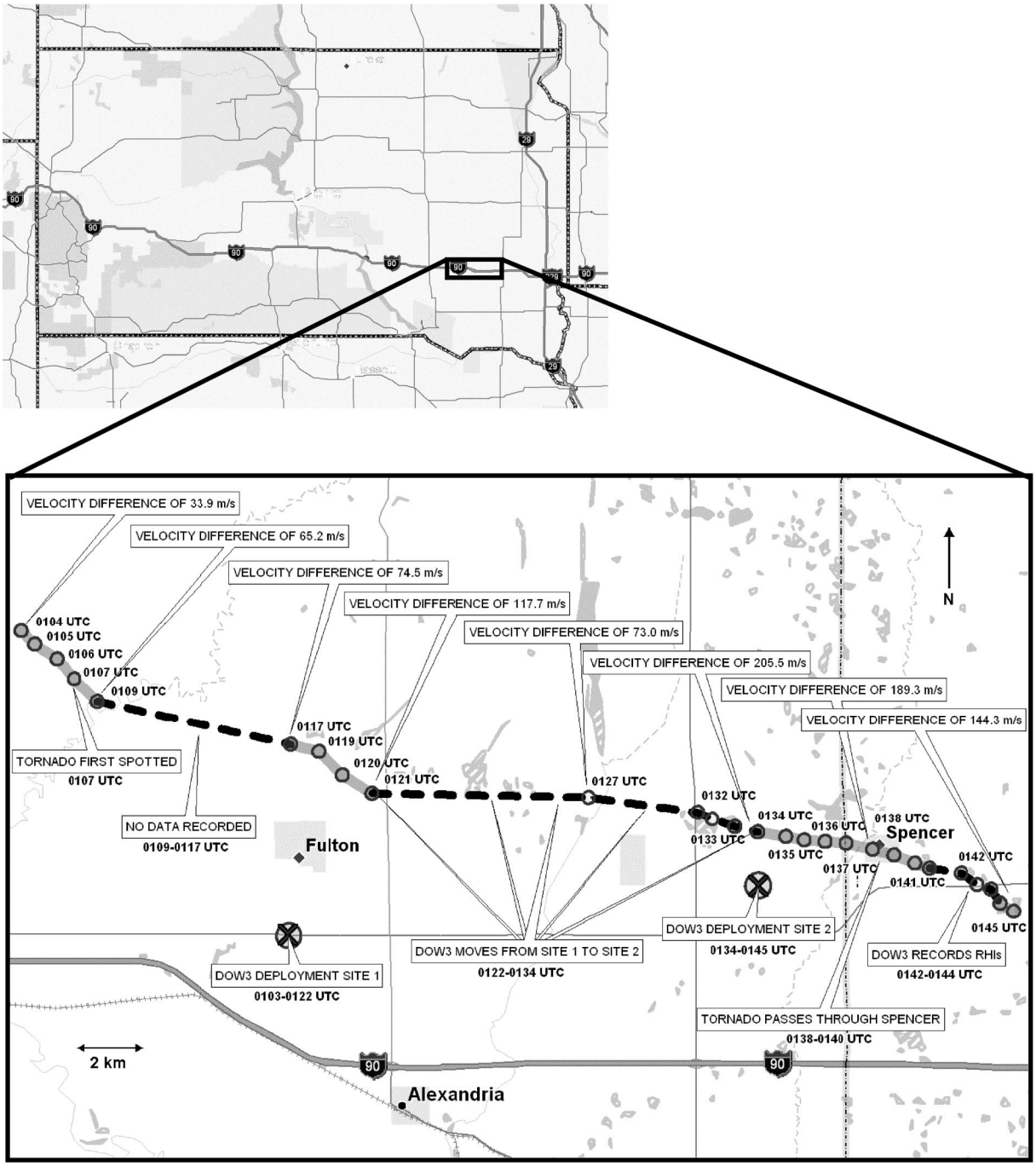

FIG. 7. A regional map of southeastern South Dakota showing the two deployment locations for DOW3 during 0103 to 0122 UTC and 0134 to 0145 UTC on 31 May 1998. The approximate tracks of the tornadoes are shown with each circle representing the position of the velocity couplet in the lowest elevation scan (usually 0.5°) of each volume. Dashed segments of the tracks represent uncertainty in the ground-relative position or existence of a tornado due to either an absence of velocity data, truck motion, or an RHI scanning strategy.

there was a gap in both the DOW and KFSD radar data, and the subcloud layer was visually obscured by dust. Therefore, it is difficult to determine conclusively whether this tornado dissipated at 0115 UTC and a second tornado developed by 0117 UTC, or whether there was simply a single tornado.

Between 0122 and 0134 UTC DOW3 moved 16 km to the east before redeploying about 4 km west-southwest of the center of Spencer (Fig. 7). During this time period, the velocity couplet near the tip of the hook echo appeared to fluctuate both in size and intensity. At 0121:19 UTC, one volume after that shown in Fig. 8d,

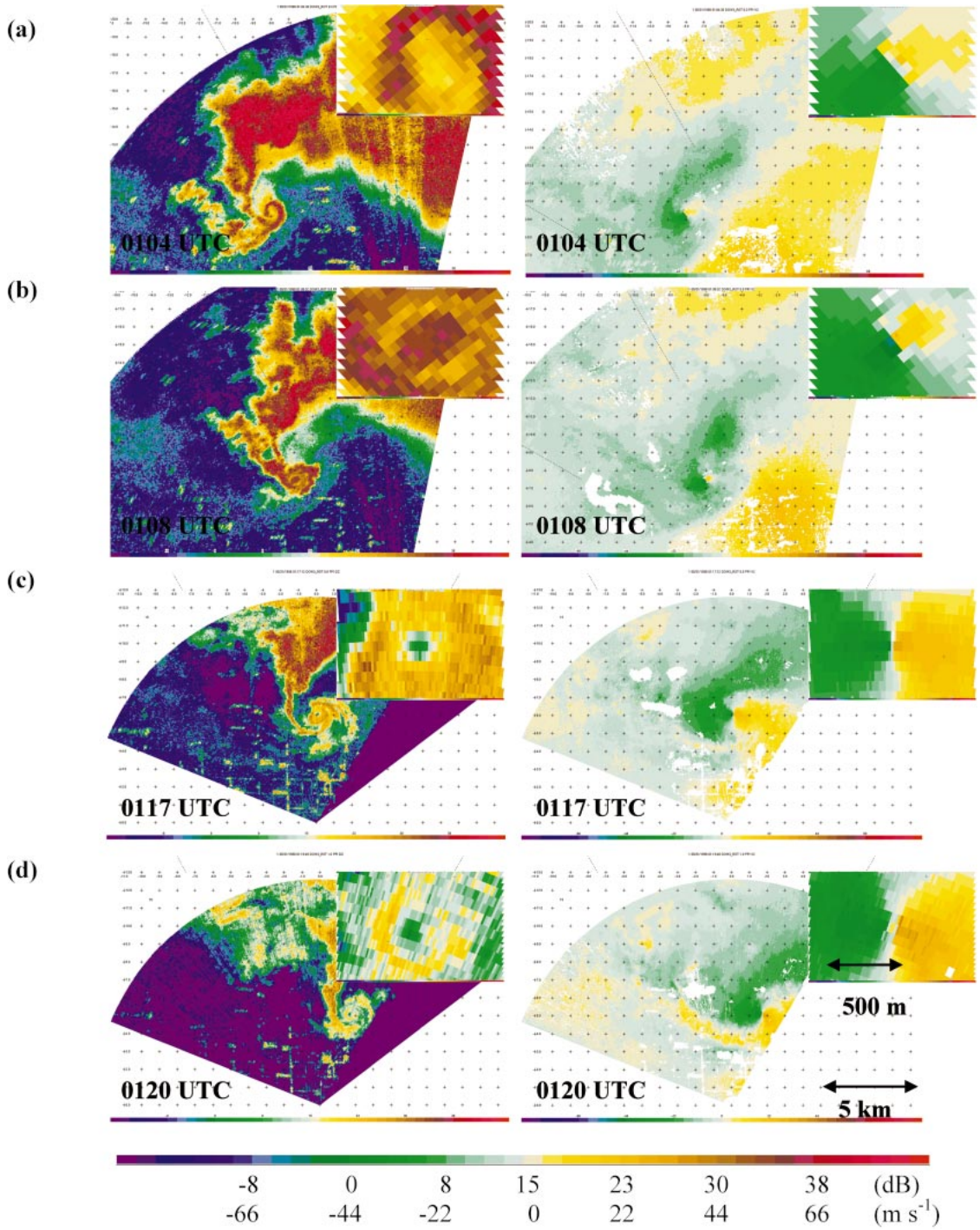

FIG. 8. The 0.5° elevation scan of the tornadic region in the supercell from DOW3 showing both (left) uncalibrated reflectivity and (right) edited Doppler velocity at (a) 0104, (b) 0108, (c) 0117, and (d) 0120 UTC. Zoomed insets in the velocity panels illustrate the wind field in the tornado itself. Irregular white areas in velocity panels represent data removed because of clutter contamination.

the low-level shear across a 150-m couplet was 110 m s^{-1} at 140 m AGL. At 0126:33 UTC the 200-m-wide velocity couplet contained 73 m s^{-1} of shear at the same altitude, increasing again to 94 m s^{-1} by 0132:03 UTC. The observed reflectivity field contained a hook echo coiled at the tip, although the coil was well separated from the core region of the supercell. This morphology is typical of well-developed, nondissipating tornadoes

FIG. 9. Video stills from the first deployment site of DOW3 along Highway 38 south of Fulton, SD, looking north-northwest as the tornado moves east-southeast at (a) 0108 UTC, when the condensation funnel first reached the ground, and (b) 0115 UTC, as the condensation funnel becomes obscured by dust and small debris (courtesy of D. Dowell).

(Wurman and Gill 2000). The NWS damage survey indicated a 1.3-km break in the damage track, and the dissipation of the second tornado was followed quickly by the formation of a third tornado between 0122 and 0123 UTC. Given the sustained strength of the low-level circulation and the reflectivity structure, it appeared there was no dissipation of the second tornado, but rather a slight weakening before reintensification by 0132 UTC.

The KFSD radar continued to observe a supercell with a large hook and well-defined mesocyclone at the lowest observed levels, about 900 m AGL, between about 0129 and 0144 UTC (Fig. 10). The forward speed of the supercell increased to almost 25 m s^{-1} between 0135 and 0155 UTC. This increase in speed may have been due in part to the formation of a linear MCS that had overtaken the supercell from the northwest by 0155 UTC. The gate-to-gate shear increased once again to about 68 m s^{-1} around 0134 UTC before slowly decreasing in strength to around 20 m s^{-1} by 0155 UTC. The two peaks in gate-to-gate shear were also followed by deviations in supercell motion of approximately 25° to the right of the forward motion about 10 min prior to each peak. The maximum gate-to-gate shear was about 60 m s^{-1} at 0139 UTC when a tornado was passing through Spencer (Fig. 10c). The KFSD MDA continued to track the mesocyclone with this storm between 0130 and 0215 UTC, while a TVS was detected between 0134 and 0144 UTC. The MDA shear reached a second and final maximum around 0129 UTC and remained steady until 0139 UTC before starting a slow but steady weakening trend, while the TVS reached a peak shear and lowest elevation at 0139 UTC (Table 1). This trend in shear is in contrast to the DOW3 observations, which indicate an earlier peak in the near-surface velocity couplet shear around 0134 UTC with a slow but steady decrease in intensity thereafter.

Between 0134 and 0145 UTC, DOW3 remained stationary and level while observing the now large and violent tornado moving east-southeast and across the town of Spencer (Figs. 11, 12). The center of the tornado was located about 1.7 km from DOW3 at 0134:27 UTC, and it moved east-southeastward at about 15 m s^{-1} toward a heading of 100°. Observations from DOW3 included a shift in wind direction from the southeast to the northwest during the passage of the rear-flank gust front between 0137 and 0138 UTC, and near-ground Doppler velocities in the rear-flank downdraft (RFD) were consistently between 15 and 20 m s^{-1}. This motion supported the conceptual model of a tornado vortex residing along the interface between the RFD and the inflow region of the supercell (Lemon and Doswell 1979). The tornado center was at its closest approach to DOW3 around 0134 UTC, and based upon the tornado's core size, rotational speed, and translational motion, the region of damaging wind speeds >40 m s^{-1} passed within 700 m of DOW3.

Video taken from 7 km east-southeast of Spencer during this time period also confirmed the presence of a large tornado with a broad condensation funnel and associated debris field (Fig. 13). A lowering in the cloud base associated with an updraft was observed immediately to the north of the tornado while a sharp vertical edge was visible in the parent wall cloud just to the south of the tornado. At approximately 0140 UTC the tornado was exiting the southeast side of Spencer and the base of the tornado debris cloud was about 600 m wide or roughly one and a half times the distance between the peak inbound and outbound Doppler velocities as measured from DOW3 (Fig. 14a).

The spatial and temporal resolution of the velocity and reflectivity data over Spencer from DOW3, located only 4 km from the center of the town, is considerably higher than that of the nearest WSR-88D located in Sioux Falls, approximately 72 km from Spencer. The elevation difference between the DOW's location and Spencer was only a few meters, and the curvature effect of the earth's surface is less than 1 m over the distance between the radar and the town. This geometry results in the centerline position of DOW3 radar beams being about 30 m AGL over Spencer at the lowest elevation angle of 0.5°.

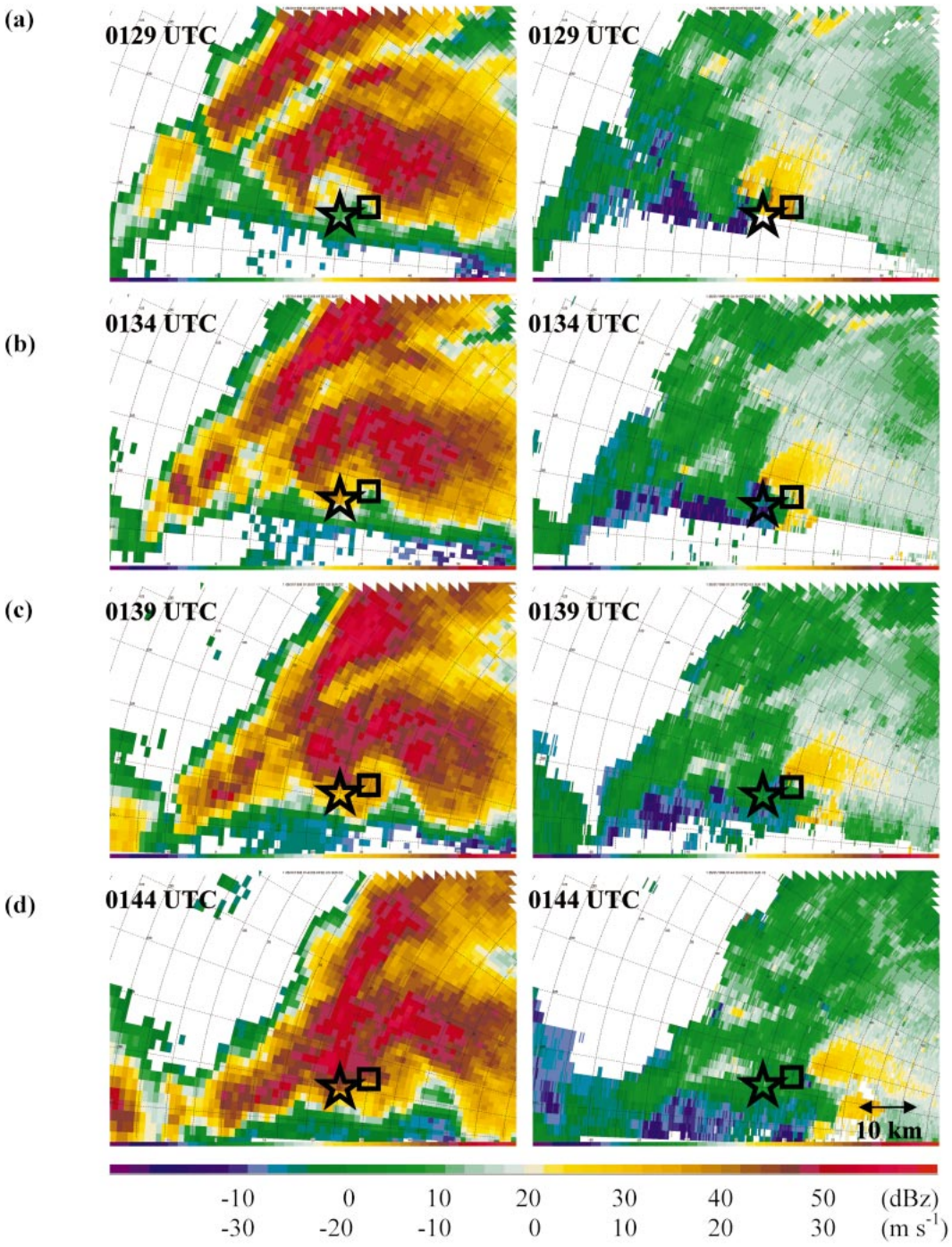

FIG. 10. The 0.5° elevation scan of the supercell from KFSD showing both (left) base reflectivity and (right) edited Doppler velocity at (a) 0129, (b) 0134, (c) 0139, and (d) 0144 UTC. The star and square represent the approximate locations of DOW3 during its second deployment and Spencer, respectively.

It is important to note that DOW elevation angles are carefully corrected for truck bed and antenna pedestal mounting tilt, and the truck is leveled using precise hydraulic load levelers, resulting in total elevation pointing errors of less than 0.2°. Furthermore, partial blockage by trees and other features can be detected due to reduced return power compared to scans immediately above, and the affected data are deleted. Fortunately, this was an infrequent problem in this dataset and did not affect the data even over Spencer itself, which was behind a low grove of trees.

Because of the large horizontal distance and elevation

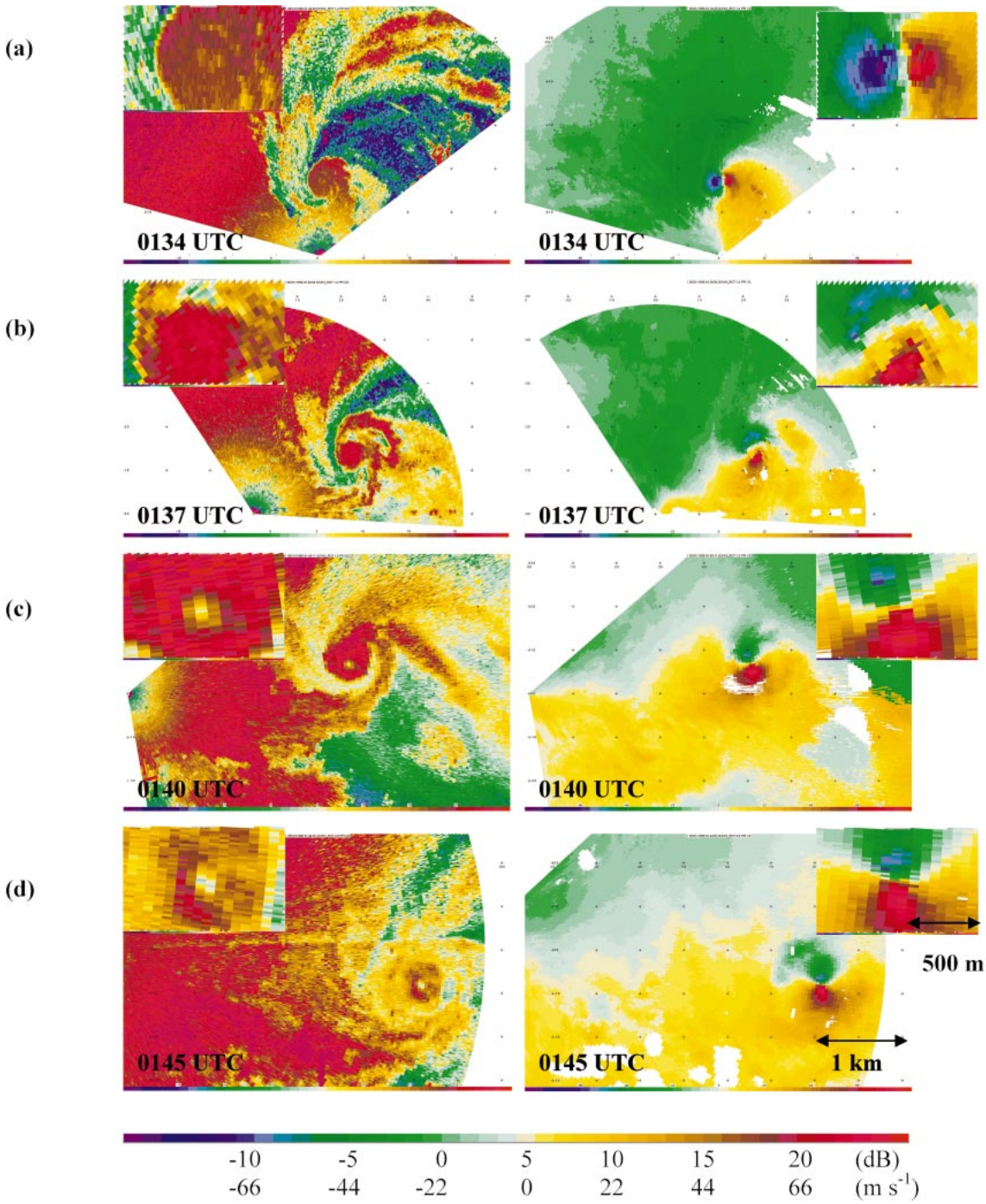

FIG. 11. The 0.5° elevation scan of the tornadic region in the supercell from DOW3 showing both (left) uncalibrated reflectivity and (right) edited Doppler velocity at (a) 0134, (b) 0137, (c) 0140, and (d) 0145 UTC. Zoomed insets in the velocity panels illustrate the wind field in the tornado itself. Note that the reflectivity values near the radar are spuriously reduced because of receiver saturation.

differences between the WSR-88D and Spencer, the centerline of the KFSD radar beams at the lowest elevation angle of 0.5° are about 925 m AGL when incorporating the curvature effect and assuming the refractive effects of a standard atmosphere. Therefore, the WSR-88D is likely measuring Doppler velocities above cloud base (Fig. 14b). In Part II a more detailed analysis of this radar geometry is performed when examining the tornado damage in Spencer.

DOW3 continued to scan the tornado to the east, after it exited Spencer, and took three volumes of vertical scans (RHIs) through the tornado between 0142 and

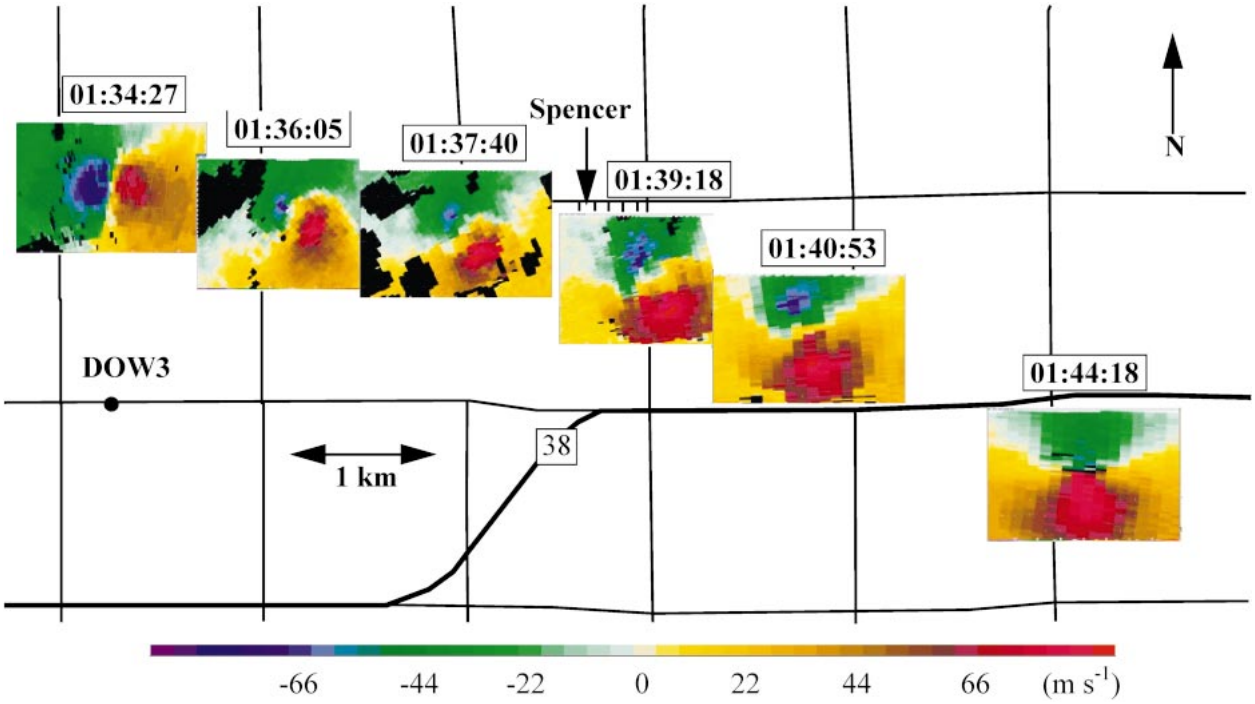

FIG. 12. Navigated Doppler velocity field (m s^{-1}) from DOW3 showing the geographic location and size of the tornado velocity couplet in the 0.5° elevation scan for every other radar volume between 0134 and 0145 UTC. The road map of the local region is displayed in the background.

0145 UTC. While others have reported vertical slices through tornadic storms and intense 1–2-km-scale reflectivity and velocity features (Fujita 1992; Wakimoto et al. 1996; Wakimoto and Atkins 1996), the radar scans reported here are an order of magnitude finer in scale and represent the first ever capable of resolving the 200–600-m-scale core flow of a tornado and the innermost clear eye region with the prerequisite 6–10 independent samples across the feature of interest (Gal-Chen and Wyngaard 1982; Carbone et al. 1985). The cross sections reveal strong differential velocities in a vertical column collocated with a vertical tube containing a minimum in reflectivity approximately 30 dB lower than the surrounding region (Fig. 15). The shifting elevation of differential velocities in adjacent vertical scans with an azimuthal angle separation of 2° show the tornado vortex was inclined about 20° toward the north from the vertical. This tilt was oriented toward the parent mesocyclone above cloud base and is consistent with observations from the 1995 Dimmitt, Texas, tornado (Wurman and Gill 2000). This tilt in the vortex produces the differential velocities because the radar beam is actually sampling opposing sides of the vortex at different elevations. The vortex tilt at this time may be due in part to the rear-flank downdraft, which is surging outward and overtaking the tornado's position (Fig. 11c).

After the series of vertical scans, the DOW resumed normal volumetric scanning. The hook echo present at 0145 UTC (Fig. 11d) is more fully coiled and the tornado circulation is considerably less separated from the main core of the supercell. This is typical of the dissipation phase of a tornado, and in fact this tornado did weaken and dissipate shortly thereafter. DOW3 undeployed shortly after 0145 UTC and concluded its observations of the tornado and parent supercell. Further intercepts were impossible because of near-zero visibility in the rear-flank downdraft.

FIG. 13. Video still from along Highway 38 about 7 km east-southeast of Spencer looking west-northwest as the tornado moves east-southeast just after 0136 UTC when the tornado was near its peak intensity (courtesy of M. Lisius).

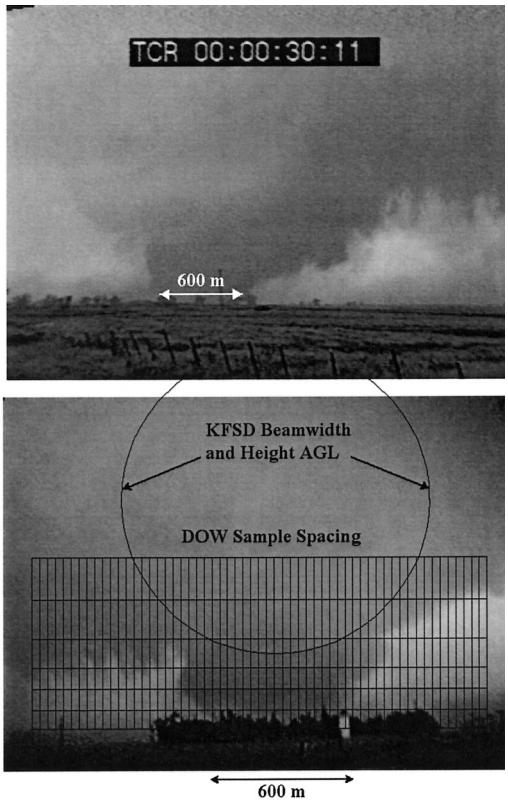

FIG. 14. Video stills just after 0140 UTC as the tornado was exiting Spencer (a) from along Highway 38 about 7 km east-southeast of Spencer looking west-northwest (courtesy of M. Lisius) and (b) from about 4 km west-southwest of Spencer looking east-northeast from the second DOW deployment site (courtesy of D. Dowell). The estimated width of the debris cloud just above the tree line was about 600 m. This debris cloud width was approximately one and a half times the diameter of the core in the tornado at this time, and about the same width as the high-reflectivity disk. The approximate size and position of the KFSD WSR-88D (0.5° only) and DOW3 radar beams (range of tornado from DOW3 is 5 km) are shown for reference. The DOW3 scanning strategy employed oversampling in the horizontal but not the vertical.

5. Doppler velocity evolution

DOW observations during the periods 0103–0110, 0117–0122, 0126, 0132–0142, and 0144–0145 UTC were spread over elevations between 10–20 m and 5 km AGL with the tornado between 1.7- and 14-km range (Fig. 16). The range of observation elevations necessarily decreased with time as both the couplet and radar move closer together, resulting in asymmetric vertical sampling. Therefore the higher elevations of the tornado vortex remain unobserved during the later periods when the tornado appeared most intense.

The time evolution of the Doppler velocity couplet in the tip of the hook echo revealed a pronounced increase in the peak velocity difference across the couplet (hereinafter referred to as the Delta-V). The three successive observation periods, roughly 0100–0115, 0115–0130, and 0130–0145 UTC, have average Delta-Vs of 54, 77, and 139 m s^{-1}, with standard deviations of 10, 17, and 21 m s^{-1}, respectively (Fig. 17a). This trend in the average Delta-V clearly shows a marked increase in shear across the velocity couplet even when considering the asymmetric vertical sampling. The minimum Delta-V of 34 m s^{-1} occurs aloft during the first observation time at 0103:38 UTC, while the maximum Delta-V of 206 m s^{-1} occurs early during the final observation period at 0134:30 UTC, and both observations are within 600 m AGL. The Delta-V remains below 75 m s^{-1} above about 1500 m AGL, while the Delta-V values above 150 m s^{-1} appear to be confined to within 500 m AGL. The most extreme Delta-V values lie within 100 m AGL, with the maximum of 206 m s^{-1} observed at just 50 m AGL. This is quite consistent with what was observed in the Dimmitt tornado. It is interesting to note that above 1.5 km the mesocyclone remained at nearly constant strength in both the DOW and WSR-88D observations, with a Delta-V around 60 to 65 m s^{-1}. However, as noted before, the MSI increased significantly during the KFSD data gap ending at 0129 UTC then remained relatively constant. While there were limited DOW observations above 1.3 km after 0130 UTC, extrapolation of the Delta-V to heights above 1.5 km yielded a mesocyclone strength similar to those from the previous observation periods. It is worthwhile to note that the tornado reached its peak and relatively steady-state intensity around 0134 UTC well before the squall-line interaction discussed in Carey et al. (2003). (See separation of supercell and squall line at 0134 UTC in Fig. 10b.) Furthermore the growth to peak tornado intensity appeared poorly correlated with mesocyclone Delta-V, supercell volume over 40 dB*Z*, or lightning indicators as shown in Carey et al. (2003). Because of the gap in KFSD data until just prior to peak tornado intensity, it was impossible to determine if MSI had any predictive value.

Taking the quotient of twice-each Delta-V with the distance between peak inbound and outbound velocities values permits the estimation of the axisymmetric vertical vorticity across the couplet (hereinafter referred to AVV). The three successive observation periods have average AVVs of 0.4, 1.1, and 0.7 s^{-1} with standard deviations of 0.4, 0.7, and 0.3 s^{-1}, respectively (Fig. 17b). The AVV ranges from a minimum of 0.05 s^{-1} during the first observation at 0103:38 UTC to maximum of 2.8 s^{-1} at 0117:17 UTC early in the second observation period. These AVV values compare to peak values between 1.0 and 1.8 s^{-1} in the Dimmitt tornado (Wurman and Gill 2000). This AVV value is higher than any previously observed across a tornado; however, higher values have been observed in multiple vortices within a tornado (Wurman 2002). The evolution of AVV supports a conceptual model that the first tornado was relatively weak with a small core region prior to 0115 UTC, and the second tornado increased in shear intensity while maintaining a similar small core until

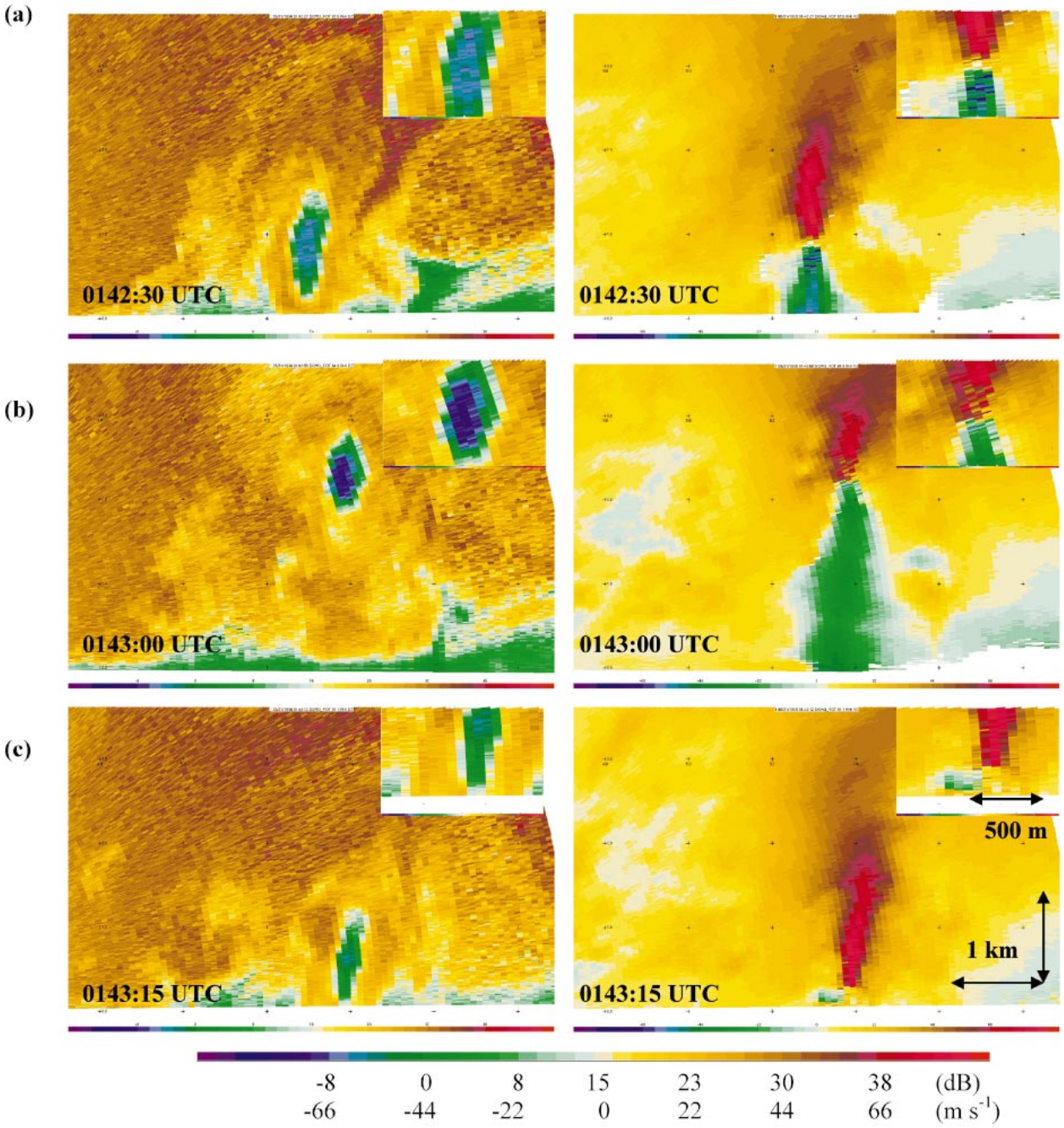

FIG. 15. Vertical scans through the tornado from DOW3 showing both (left) uncalibrated reflectivity and (right) edited Doppler velocity at (a) 0142:30 UTC through the low-level core flow, (b) 0143:00 UTC north of the low-level core flow, and (c) 0143:15 UTC through the near-surface eye. All RHIs are taken within a few degrees of due east shortly after the tornado passed through Spencer. The position of differential velocities in a vertical column on adjacent RHIs indicates that the tornado vortex is inclined at approximately 20° toward the north with increasing height during this period.

after 0130 UTC when the core grew more rapidly and the shear intensity peaked.

The AVV remains below about 0.5 s^{-1} above 1500 m AGL while the AVV values above 1.5 s^{-1} mostly reside below 500 m above the surface. The extreme AVV of 2.8 s^{-1} is observed at only about 90 m AGL. These observations clearly demonstrate the unfortunate reality that the portion of a tornado and parent supercell most likely to go unobserved by conventional Doppler radar also contains the most intense wind speeds posing the largest threat to loss of life and property.

When viewing the velocity couplet observations as

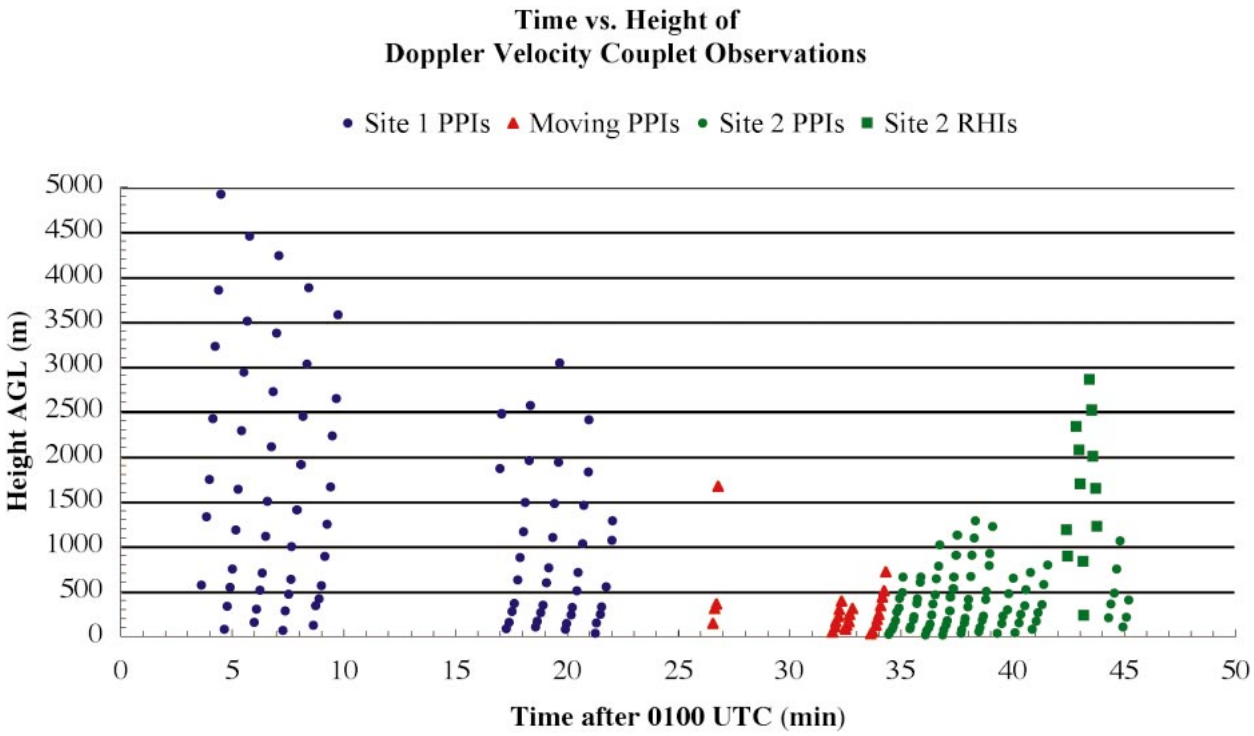

FIG. 16. The height above ground level of the DOW3 measurements of the Doppler velocity couplet. The range to the center of the Doppler velocity couplet from DOW3 varied from 1.7 to 14.0 km during this time period.

both a function of height and time it is possible to track the 2D evolution of the Delta-V and AVV (Fig. 18). The Delta-V appears to increase almost uniformly in the lowest 5 km from 40 to 70 m s^{-1} during the time of the first tornado between 0103 and 0109 UTC (Fig. 18a). AVV greater than 0.6 s^{-1} near the ground at 0104 UTC is associated with a small core-flow diameter that increases at later times, reducing AVV. During the early stages of the second tornado, the larger shear values over 100 m s^{-1} become concentrated within about 500 m AGL from 0117 to 0126 UTC. As the second tornado approaches its peak intensity just above surface around 0132 UTC the Delta-V undergoes a quasi-periodic intensity oscillation within a few hundred meters AGL. The oscillations have a period of about 120 s and produce shear fluctuations between 20 and 30 m s^{-1}, thereby modulating the strongest near-surface shear between about 150 and 190 m s^{-1} over the time between 0132 and 0140 UTC. This may be indirect evidence of a multiple-vortex structure in the tornado.

Isolated sweeps, none near the ground, show more direct evidence of multiple-vortex structure. At 0136:27 UTC and 8.0° elevation, the reflectivity of the disk of debris contained several minima or eyes characteristic of multiple vortices (Fig. 19) that were estimated to have amplitudes of approximately 30 m s^{-1} by Wurman (2002). Very strong wind shears were associated with these multiple eyes, suggesting that multiple vortices exhibiting wind field perturbations of significantly less magnitude than the main tornado circulation existed. Since these features did not exhibit sweep-to-sweep continuity, it is not possible to document thoroughly the multiple-vortex behavior in this tornado. It is likely that the 120-s period oscillation in shear is a highly aliased artifact of the progression of weak multiple vortices around the tornado. The revolution period of an individual multiple vortex located at the edge of the core-flow region and moving at approximately one-half of the rotational speed of the tornado (Wurman 2002) would be approximately 120 s.

The AVV also exhibits some unique 2D evolution. The first tornado appears to have the highest vorticity. Values over 1.0 s^{-1} develop aloft between about 500 and 1500 m AGL between 0103 and 0109 UTC (Fig. 18b). However, during the early stages of the second tornado, the highest vorticity values become concentrated closer to the surface within about 500 m AGL with peak values over 2.0 s^{-1} at the surface between 0117 and 0120 UTC. By the final time period between 0132 and 0145 UTC the high vorticity values over 1.0 s^{-1} appear concentrated within about 200 m AGL while there is a reduction of vorticity aloft from 1.0 s^{-1} at earlier periods to nearly half this value at 1000 m AGL.

The uncalibrated reflectivity field in the tornado's core revealed a unique observation in this same 2D framework. A minimum in reflectivity or ''eye'' at the center of the core appeared to descend rapidly toward the ground as the tornado passed through Spencer between

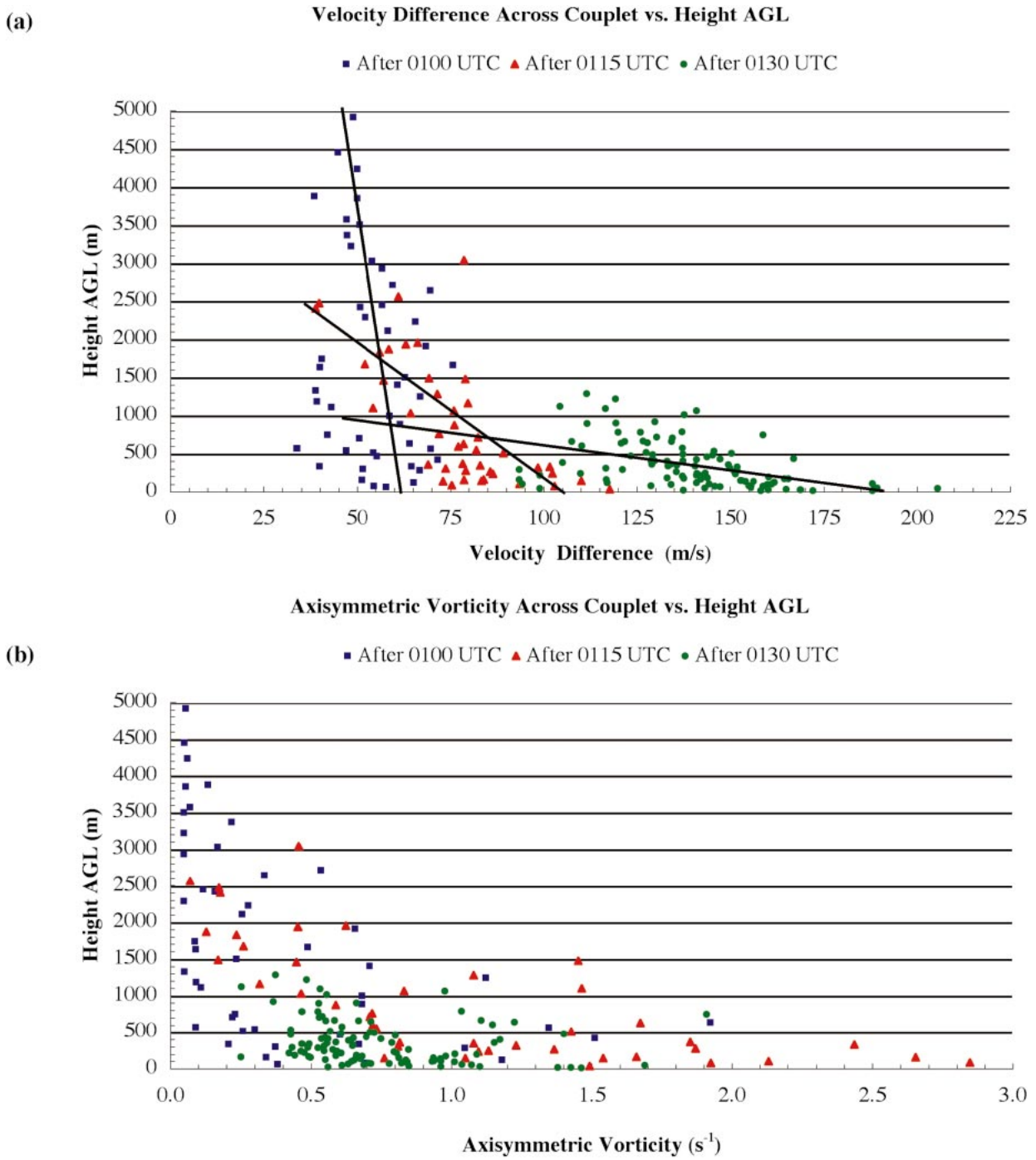

FIG. 17. The (a) peak velocity difference including a linear regression line for each time period and (b) axisymmetric vorticity across the tornado as a function of height above ground level.

0138 and 0140 UTC (Fig. 20). The 0-dB isopleth descends from about 1 km AGL to near the surface between 0137 and 0141 UTC. The exact cause for this change is uncertain, but centrifuging from the introduction of large debris or a structural change in the tornado such as the formation of a central downdraft could explain this observation (Dowell et al. 2004).

6. Comparison of tornado and mesocyclone evolution at low levels

In an attempt to compare the evolution of the wind field close to the ground and near cloud base, the lowest tilt (usually 0.5°) of each radar volume from DOW3 and KFSD were used to characterize the tornado and mesocyclone wind fields, respectively. Before 0130 UTC

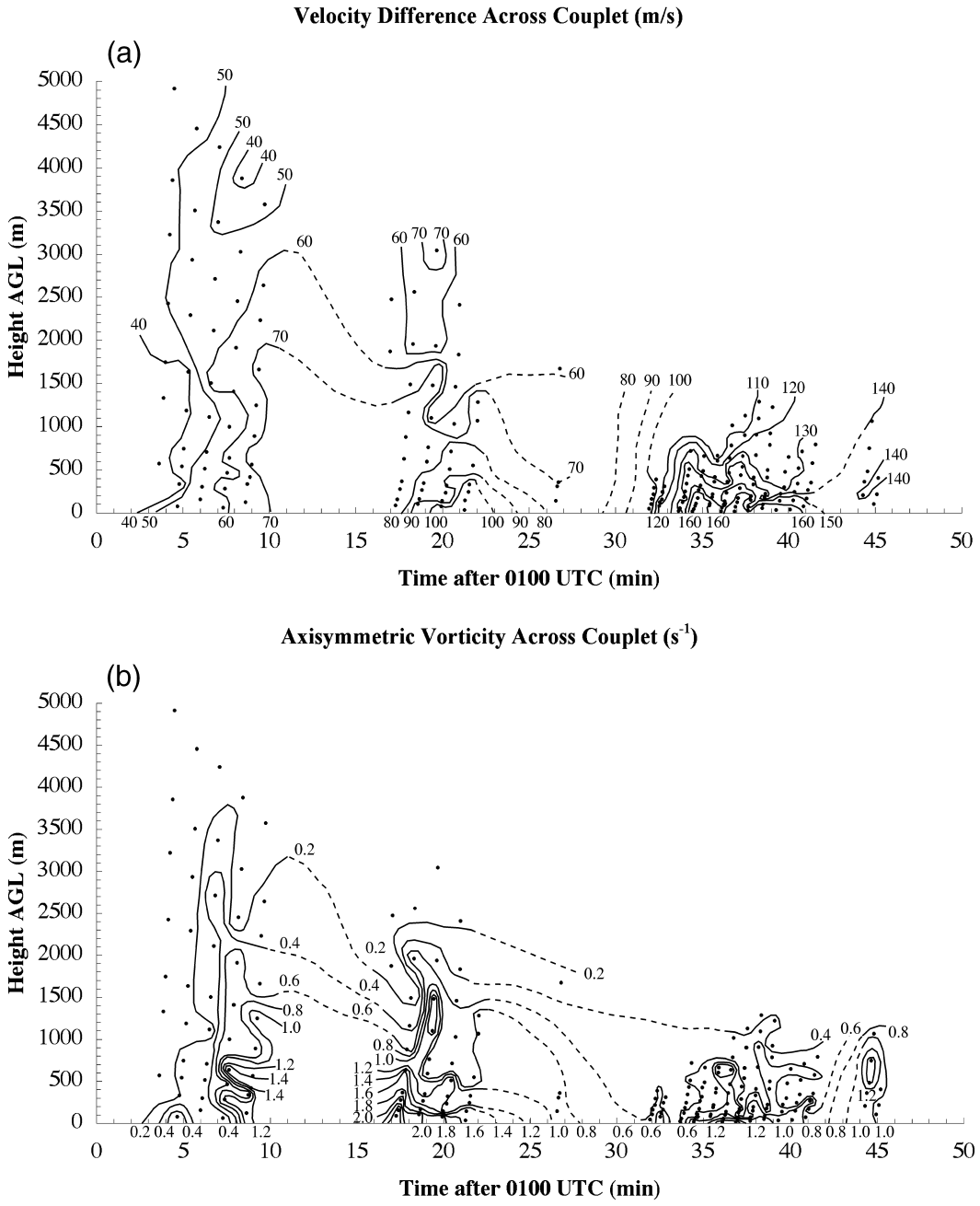

FIG. 18. The (a) peak velocity difference and (b) axisymmetric vorticity across the tornado as a function of time and height.

the centerline of the lowest DOW3 radar beams remained below 200 m AGL as the range to the velocity couplet center slowly decreased from about 13 km at 0103 UTC to just under 6 km by 0122 UTC. The centerline of the radar beam was below 100 m AGL for 10 of the 11 0.5° elevation scans during the final observation period, and below 40 m AGL when the tornado was passing through Spencer. The KFSD radar beam centerline remained at or above 600 m AGL as the range to the mesocyclone slowly decreased from about 110-km range at 0045 UTC to about 55 km at 0150 UTC (Figs. 21a,b).

The distance between the peak inbound and outbound DOW Doppler velocities in the tornado's rotational couplet was between 50 and 100 m for the first tornado. The core diameter increased to 250 m early in the life of the second tornado before further increasing in size to between 300 and 350 m while the tornado was passing through Spencer, and eventually to 400 m by 0141 UTC before slowly decreasing in size thereafter. Core di-

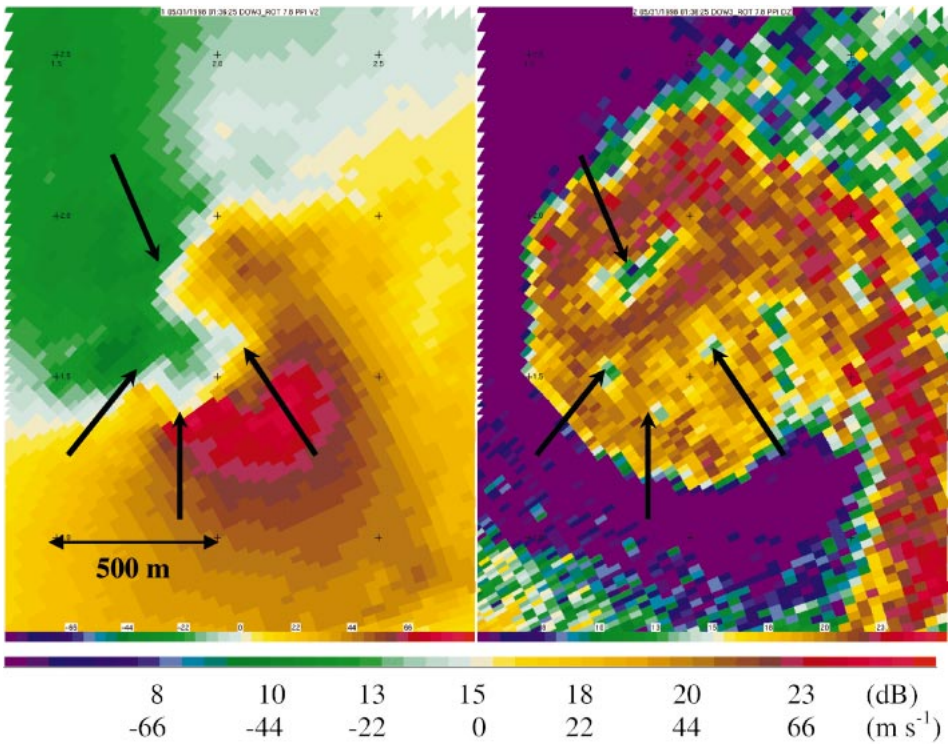

FIG. 19. The DOW 7.5° elevation scan at 0136:27 UTC showing (left) edited Doppler velocity and (right) uncalibrated reflectivity through the tornado at about 360 m AGL and 2.4-km range. The tornado exhibits its largest observed departure from axisymmetry at this time and contains several regions of locally enhanced shear and reflectivity minimums (arrows).

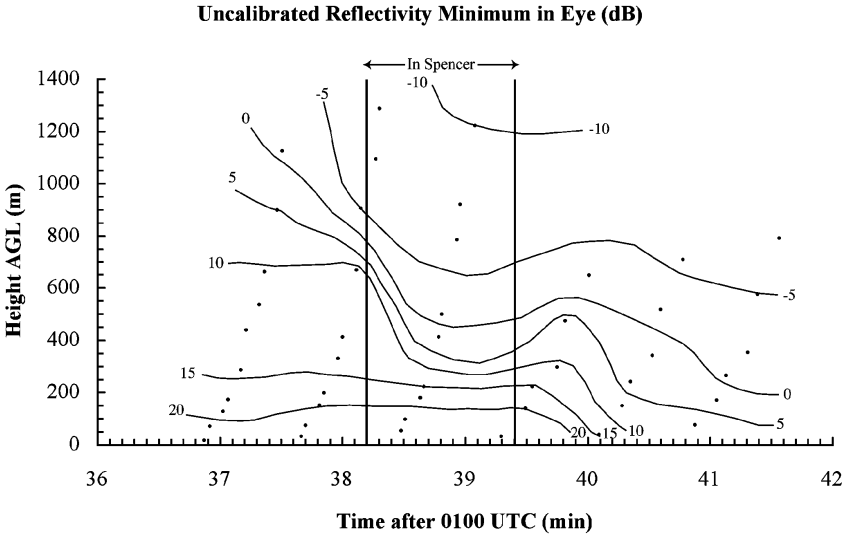

FIG. 20. The evolution of the uncalibrated reflectivity field (dB) as a function of height AGL. The heights AGL of the tornado center at the time of every elevation scan between about 0137 and 0142 UTC are represented by points. Actual reflectivity values in the eye at the earliest times may have been even higher than shown but could not be measured because of receiver saturation due to the extremely close range of the tornado to the radar. The time interval during which the tornado's low-level core-flow region is at least partially in Spencer is contained within the vertical lines.

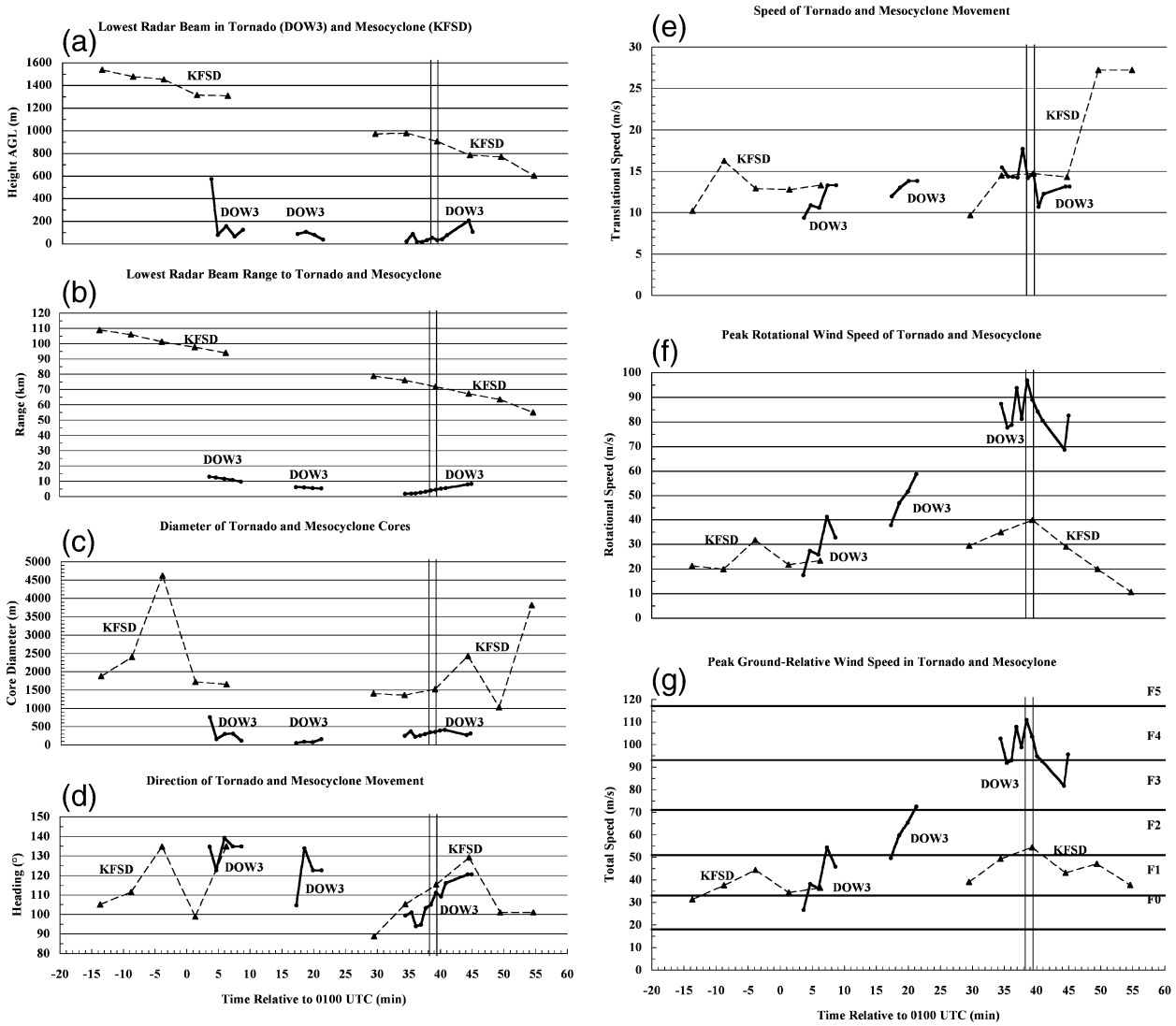

FIG. 21. Evolution of the Doppler velocity couplet from the lowest elevation scan for each radar volume (usually 0.5°) from both DOW3 and KFSD between 0040 and 0200 UTC including (a) height AGL (m) of the radar-beam centerline at the center of the velocity couplet; (b) range to the center (km) of the velocity couplet; (c) distance between peak inbound and outbound Doppler velocities or twice the radius of maximum winds, R(m); (d) estimated bearing, β(°), of the velocity couplet center; (e) estimated translational speed, V_t(m s^{-1}), of the velocity couplet center; (f) the estimated maximum rotational wind speed, V_{rm}(m s^{-1}), from the average of the peak inbound and outbound Doppler velocities after the removal of the translational component; and (g) the maximum ground-relative wind speed combining both the rotational and translational wind components. The threshold wind speed for each Fujitas scale category is shown for reference in the total wind speed, and the time during which the vortex core was in Spencer is bracketed by the vertical lines in (a)–(g).

ameter of the low-level mesocyclone as viewed by KFSD exhibited less of this trend and remained near 2 km on average through most of the observation period (Fig. 21c).

The DOW-measured tornado maintained an east-southeastward motion with a heading varying from 95° to 140° and a forward speed between 10 and 15 m s^{-1}, very similar to the mesocyclone motion measured from KFSD (Figs. 21d,e). During the intensification periods of both observed tornadoes, the mesocyclone appeared to move up to 30° to the right of the motion observed during the weaker tornadic or nontornadic time periods.

By subtracting the observed component of translational motion in the velocity couplet, an estimate of the rotational speed in the couplet is obtained for both the maximum inbound and outbound sides of the tornado and mesocyclone. The average of these estimates for the early time periods of the DOW observations revealed an increasing rotational speed from about 17 m s^{-1} at 0103 UTC to nearly 60 m s^{-1} by 0122 UTC (Fig. 21f). During the second tornado, the estimated peak rotational velocity ranged from a high of 97 m s^{-1} at 0138:29 UTC to a low of 69 m s^{-1} at 0144:18 UTC. The mesocyclone observed by KFSD revealed an es-

timated average rotational speed between 20 and 40 m s^{-1} during most of the observation period.

On the right side of the tornado wind field relative to the direction of translation, the rotational and translational components of the wind field should be additive for a cyclonic vortex, and this resulted in estimates of the peak instantaneous ground-relative wind speed in the velocity couplet. For the early DOW observations periods, the estimated peak wind speed slowly increased from 27 m s^{-1} at 0103 UTC to 77 m s^{-1} by 0122 UTC (Fig. 21g). During the final DOW observation period the estimated peak wind speed, using the aforementioned averaging method varied between 111 m s^{-1} at 0138:29 UTC and 82 m s^{-1} at 0144:18 UTC. During the period when the tornado was passing through Spencer, the estimated total wind speed was in the range between 105 and 110 m s^{-1}, which was well into the range considered capable of causing F4 damage (Fujita 1971). The strongest mesocyclonic ground-relative motion of 54 m s^{-1} was coincident with the strongest estimated tornado ground-relative motion of 111 m s^{-1} between 0138 and 0139 UTC. Note that because of asymmetries in the tornado structure, actual estimated peak wind speeds were as high as 118 m s^{-1}, barely into the F5 range, just prior to the tornado passing through Spencer.

Between, 0134:30 and 0136:52 UTC, the peak Doppler velocities in the lowest elevation angle increased to a maximum of 104 m s^{-1} at 0136:52 UTC before slowly decreasing thereafter. This Doppler velocity maximum compares to DOW radar observations of strong tornadoes near Dimmitt, Texas (2 June 1995); Mulhall, Oklahoma; and Bridge Creek, Oklahoma (3 May 1999), where peak near-ground Doppler velocities (not compensating for unobserved components) reached a maximum of 74, 109, and 134 m s^{-1}, respectively (Wurman and Gill 2000; Wurman 2002). (In the latter case, ground-relative winds were 135 m s^{-1}.)

7. Low-level convergence

Examination of the Doppler velocities in the lowest portions of the vertically oriented RHI scans obtained between 0142 and 0144 UTC suggests the existence of strong near-surface convergence. Below 100 m AGL, Doppler velocities on the side of the tornado nearest the radar are as high as 30 m s^{-1} away from the radar, while velocities on the far side of the tornado are 4 m s^{-1}. After removing the translational component, this implies an inward component of motion of 13 m s^{-1}, which compares favorably with other independent calculations of inward motion in this tornado at a different time (Dowell et al. 2005). The maximum velocity difference in the radial direction through the core divided by the core diameter is 0.03 s^{-1}, implying convergence of twice that value, or 0.06 s^{-1}. It is possible that the low outbound velocities on the far side of the tornado were a result of contamination from ground clutter, but the strong outward velocities on the near side of the tornado, approximately twice the translational motion of the tornado, imply that convergence of at least half of the above-calculated value was present. Furthermore, as described above, data that were clearly contaminated by ground clutter were deleted prior to further analysis. Asymmetries in the tornadic flow, possibly caused by multiple vortices, could also have contaminated this calculation. Further evidence of surface layer convergence in the tornado is suggested by the weakening of winds at 19 m AGL compared to values observed just above. A 172 m s^{-1} Doppler velocity difference across the tornado at 19 m AGL (the level of the lowest scan) during the tornado's closest approach to DOW3 at 0134:27 UTC was 34 m s^{-1} less than the difference of 206 m s^{-1} observed immediately above it. Further discussion of winds in the extreme lowest levels of the tornado is presented in Part II.

8. Conclusions

Favorable synoptic and mesoscale atmospheric conditions on the evening of 30 May 1998 supported a severe weather event across southeastern South Dakota. Abundant low-level moisture, steep midlevel lapse rates, and sufficient deep-layer shear were all present in close proximity to an upper-level jet streak. Several surface boundaries including a cold front and a dryline interacted with these conditions and produced severe moist convection including a violent tornadic supercell despite the lack of strong low-level shear in the local environment.

The parent supercell and associated tornadoes that moved across southeastern South Dakota and through Spencer, South Dakota, on 30 May 1998 were observed visually and by both a DOW mobile radar and the KFSD WSR-88D. The visual observations of the tornadoes were occasionally obscured by dust, while some gaps are present in the DOW and WSR-88D radar data either due to beam blockage, operator error, or movement of the DOW radar. A lack of damage descriptors in the rural terrain reduced the effectiveness of the damage survey. Therefore, each of these independent observations contains an incomplete sampling of the tornadic supercell's evolution.

Several key differences in the observations reveal the importance of incorporating high-resolution radar data in characterizing the evolution of a tornado's structure. Particularly important tornado descriptors include the peak wind speeds, size of core diameter, and the ground-relative path locations:

(a) The DOW radar detected a near-surface rotation of the strength and scale of a tornado with winds exceeding 35 m s^{-1} in a 150-m-diameter core approximately 180 s prior to the first visual confirmation of a tornado debris cloud at the surface. Therefore, potentially damaging surface winds in a

tornado may precede the appearance of a low-level debris cloud or exist in its absence if the tornado is occurring over wet terrain or fields that have not been plowed.

(b) The damage survey revealed several gaps in the damage path of tornadoes produced by the supercell. With the lack of damage indicators in the rural region, the natural conclusion was to interpret the damage gaps as breaks between the tracks of different tornadoes, and five separate but sequential tornadoes were attributed to the observed damage pattern. While DOW Doppler velocity data were not collected over the entire domain of these damage paths, there was enough evidence in the velocity data to conclude the that a 1.3-km gap in damage between the second and third tornadoes corresponding to a time between 0122 and 0123 UTC should not have been attributed to the dissipation of one tornado and the formation of another. The DOW velocity data did reveal a brief weakening of the near-surface shear across the tornado core from 110 to 73 m s^{-1} while the core broadened from about 150 to 200 m between 0122 and 0126 UTC. However, this weakening does not support the total dissipation of the tornado's circulation, so the second and third damage tracks appear to result from a single tornado. Part II of this paper addresses the comparison of structural damage in Spencer to Doppler velocities in more detail.

(c) The time–height evolution of the Doppler velocity couplet as observed by DOW3 between 0100 and 0200 UTC revealed a gradual concentration of higher vertical vorticity within a few hundred meters AGL, with an order of magnitude increase in vorticity from near 0.2 to over 2.0 s^{-1} and a corresponding weakening of the vorticity across the couplet at higher elevations over this same time period. The shear across the tornado velocity couplet develops an oscillatory character during the most intense period of the second tornado between 0132 and 0140 UTC. This oscillation of shear magnitude of between 20 and 30 m s^{-1} is confined to within about 500 m AGL and exhibits a period of about 120 s. DOW volumetric update times of 45–50 s were too infrequent to directly relate these observations to individual multiple vortices. However, Part II suggests that a causal relationship exists between these wind field oscillations and modulations in the damage pattern. Pronounced changes in the reflectivity of the tornado core also occur during the period of these oscillations and may be the result of fundamental changes in the tornado's structure.

(d) The variations of tornado wind speed as a function of height are most pronounced in the lowest 200 m AGL, with the most extreme speeds contained just below 50 m AGL. There are suggestions that winds speeds may decrease in magnitude below 30 m AGL. Current radar observations are unable to determine the exact elevation and magnitude of the true peak in tornado wind speeds, which appear to occur between the surface and 50 m AGL. Vertical cross sections revealed the presence of strong convergence in the lowest levels of the tornado.

Acknowledgments. This work was supported in part by National Science Foundation (NSF) Grant ATM-9703032. The DOWs are operated by the Center for Severe Weather Research (CSWR) and have been developed by CSWR, the University of Oklahoma, NCAR's Atmospheric Technology Division (ATD) (which is supported by the NSF), and the National Severe Storms Laboratory. Support for the DOW program has been received from the state of Oklahoma, the NSF, the Office of Naval Research, and CSWR. David Dowell, Herbert Stein, and one of us (Wurman) crewed the DOW3 and were crucial in obtaining this dataset, collected in difficult circumstances. David Dowell and Martin Lisius provided video imagery. Mitch Randall, Jon Lutz, Jack Fox, and others at NCAR/ATD provided engineering support to develop the DOWs and to keep them running. Alan Shapiro and John Snow of OU provided scientific input and suggestions. This work was also assisted by an American Meteorological Society/NWS graduate student fellowship.

REFERENCES

Bluestein, H. B., and A. L. Pazmany, 2000: Observations of tornadoes and other convective phenomena with a mobile, 3-mm wavelength, Doppler radar: The spring 1999 field experiment. *Bull. Amer. Meteor. Soc.,* **81,** 2939–2951.

——, J. G. LaDue, H. Stein, D. Speheger, and W. P. Unruh, 1993: Doppler radar wind spectra of supercell tornadoes. *Mon. Wea. Rev.,* **121,** 2200–2221.

——, A. L. Pazmany, J. C. Galloway, and R. E. McIntosh, 1995: Studies of the substructure of severe convective storms using a mobile 3-mm-wavelength Doppler radar. *Bull. Amer. Meteor. Soc.,* **76,** 2155–2169.

Carbone, R. E., M. J. Carpenter, and C. D. Burghart, 1985: Doppler radar sampling limitation in convective storms. *J. Atmos. Oceanic Technol.,* **2,** 357–361.

Carey, L. D., W. A. Petersen, and S. A. Rutledge, 2003: Evolution of cloud-to-ground lightning and storm structure in the Spencer, South Dakota, tornadic supercell of 30 May 1998. *Mon. Wea. Rev.,* **131,** 1811–1831.

Church, C. R., and J. T. Snow, 1993: Laboratory models of tornadoes. *The Tornado: Its Structure, Dynamics, Prediction and Hazards, Geophys. Monogr.,* No. 79, Amer. Geophys. Union, 19–39.

——, ——, G. L. Baker, and E. M. Agee, 1979: Characteristics of tornado-like vortices as a function of swirl ratio: A laboratory investigation. *J. Atmos. Sci.,* **36,** 1755–1776.

Colby, F. P., Jr., 1984: Convective inhibition as a predictor of convection during AVE-SESAME II. *Mon. Wea. Rev.,* **112,** 2239–2252.

Dowell, D. C., C. Alexander, J. Wurman, and L. Wicker, 2005: Centrifuging of hydrometers and debris in tornadoes: Radar-reflectivity patterns and wind-measurements errors. *Mon. Wea. Rev.,* in press.

Fiedler, B. H., 1998: Wind-speed limits in numerically simulated

tornadoes with suction vortices. *Quart. J. Roy. Meteor. Soc.*, **124,** 2377–2392.
——, and R. Rotunno, 1986: A theory for the maximum windspeeds in tornado-like vortices. *J. Atmos. Sci.,* **43,** 2328–2340.
Fujita, T. T., 1971: Proposed characterization of tornadoes and hurricanes by area and intensity. SMRP Res. Rep. 91, University of Chicago, 15 pp.
——, 1992: *Mystery of Severe Storms.* The University of Chicago Press, 298 pp.
Gal-Chen, T., and J. C. Wyngaard, 1982: Effects of volume averaging on the line spectra of vertical velocity from multiple-Doppler radar observations. *J. Appl. Meteor.,* **21,** 1881–1890.
Lemon, L. R., and C. A. Doswell III, 1979: Severe thunderstorm evolution and mesoscale structure as related to tornadogenesis. *Mon. Wea. Rev.,* **107,** 1184–1197.
Lewellen, D. C., W. S. Lewellen, and J. Xia, 2000: The influence of a local swirl ratio on tornado intensification near the surface. *J. Atmos. Sci.,* **57,** 527–544.
Lewellen, W. S., 1993: Tornado vortex theory. *The Tornado: Its Structure, Dynamics, Prediction and Hazards, Geophys. Monogr.,* No. 79, Amer. Geophys. Union, 19–39.
——, D. C. Lewellen, and R. I. Sykes, 1997: Large-eddy simulation of a tornado's interaction with the surface. *J. Atmos. Sci.,* **54,** 581–605.
Moncrieff, M. W., and M. J. Miller, 1976: The dynamics and simulation of tropical cumulonimbus and squall lines. *Quart. J. Roy. Meteor. Soc.,* **102,** 373–394.
Nettleton, L., S. Daud, R. Neitzel, C. Burghart, W. C. Lee, and P. Hildebrand, 1993: SOLO: A program to peruse and edit radar data. Preprints, *26th Conf. on Radar Meteorology,* Norman, OK, Amer. Meteor. Soc., 338–339.
Oye, R., C. Mueller, and S. Smith, 1995: Software for radar translation, visualization, editing, and interpolation. Preprints, *27th Conf. on Radar Meteorology,* Vail, CO, Amer. Meteor. Soc., 359–361.
Rasmussen, E. N., and D. O. Blanchard, 1998: A baseline climatology of sounding-derived supercell and tornado forecast parameters. *Wea. Forecasting,* **13,** 1148–1164.
Rotunno, R., 1977: Numerical simulation of a laboratory vortex. *J. Atmos. Sci.,* **34,** 1942–1956.
——, 1979: A study in tornado-like vortex dynamics. *J. Atmos. Sci.,* **36,** 140–155.
——, 1984: An investigation of a three-dimensional asymmetric vortex. *J. Atmos. Sci.,* **41,** 283–298.
Samaras, T., 2004: Pressure measurements in a strong tornado. Preprints, *22d Severe Local Storms Conf.,* Hyannis, MA, Amer. Meteor. Soc., CD-ROM, P11.4.
USDOC, 1998: Service assessment: Spencer, South Dakota, tornado May 30, 1998. NOAA/NWS, 18 pp.
Wakimoto, R. M., and N. T. Atkins, 1996: Observations on the origins of rotation: The Newcastle tornado during VORTEX 94. *Mon. Wea. Rev.,* **124,** 384–407.
——, W.-C. Lee, H. B. Bluestein, C.-H. Liu, and P. H. Hildebrand, 1996: ELDORA observations during VORTEX 95. *Bull. Amer. Meteor. Soc.,* **77,** 1465–1481.
Ward, N. B., 1972: The exploration of certain features of tornado dynamics using a laboratory model. *J. Atmos. Sci.,* **29,** 1194–1204.
Weisman, M. L., and J. B. Klemp, 1982: The dependence of numerically simulated convective storms on the vertical wind shear and buoyancy. *Mon. Wea. Rev.,* **110,** 504–520.
Winn, W., S. Hunyady, and G. Aulich, 2000: Electric field at the ground in a large tornado. *J. Geophys. Res.,* **105** (D15), 20 145–20 153.
Wurman, J., 1996: Fine-scale Doppler radar observations of tornadoes. *Science,* **272,** 1774–1777.
——, 1999: Preliminary results from the Radar Observations of Tornadoes and Thunderstorm Experiment (ROTATE-98/99). Preprints, *29th Conf. on Radar Meteorology,* Montreal, QC, Canada, Amer. Meteor. Soc., 613–616.
——, 2001: The DOW mobile multiple-Doppler network. Preprints, *30th Conf. on Radar Meteorology,* Munich, Germany, Amer. Meteor. Soc., 95–97.
——, 2002: The multiple-vortex structure of a tornado. *Wea. Forecasting,* **17,** 473–505.
——, and S. Gill, 2000: Finescale radar observations of the Dimmitt, Texas (2 June 1995), tornado. *Mon. Wea. Rev.,* **128,** 2135–2164.
——, and T. Samaras, 2004: Comparison of in-situ pressure and radar velocity measurements in a tornado, Preprints *22d Severe Local Storms Conf.,* Hyannis, MA, Amer. Meteor. Soc., CD-ROM, 15.4.
——, and C. R. Alexander, 2005: The 30 May 1998 Spencer, South Dakota, storm. Part II: Comparison of observed damage and radar-derived winds in the tornadoes. *Mon. Wea. Rev.,* **133,** 97–119.
——, J. M. Straka, and E. N. Rasmussen, 1996: Preliminary radar observations of the structure of tornadoes. Preprints, *18th Conf. on Severe Storms,* San Francisco, CA, Amer. Meteor. Soc., 17–22.
——, ——, ——, M. Randall, and A. Zahrai, 1997: Design and deployment of a portable, pencil-beam, pulsed, 3-cm Doppler radar. *J. Atmos. Oceanic Technol.,* **14,** 1502–1512.